PB83-111633

Tire Energy Dissipation Determination

Pennsylvania Transportation Inst.
University Park

Prepared for

Environmental Protection Agency
Cincinnati, OH

Jul 82

U.S. Department of Commerce
National Technical Information Service
NTIS

PB83-111633

TIRE ENERGY DISSIPATION DETERMINATION

FINAL REPORT

SUBMITTED TO

UNITED STATES ENVIRONMENTAL PROTECTION AGENCY

THE PENNSYLVANIA TRANSPORTATION INSTITUTE
THE PENNSYLVANIA STATE UNIVERSITY
UNIVERSITY PARK, PENNSYLVANIA 16802

JULY 1982

THE PENNSYLVANIA TRANSPORTATION INSTITUTE
THE PENNSYLVANIA STATE UNIVERSITY

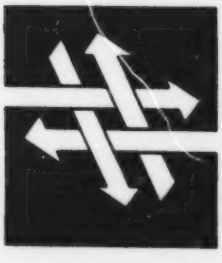

REPRODUCED BY
NATIONAL TECHNICAL
INFORMATION SERVICE
U.S. DEPARTMENT OF COMMERCE
SPRINGFIELD, VA. 22161

TECHNICAL REPORT STANDARD TITLE PAGE

1. Report No.	2. Government Accession No.	3. Recipient's Catalog No. PB83 111633
4. Title and Subtitle: TIRE ENERGY DISSIPATION DETERMINATION		5. Report Date: July 1982 6. Performing Organization Code
7. Author(s): Gordon F. Hayhoe		8. Performing Organization Report No.: PTI 8212
9. Performing Organization Name and Address: The Pennsylvania Transportation Institute The Pennsylvania State University University Park, Pa. 16802		10. Work Unit No. 11. Contract or Grant No.: 63-03-2763 13. Type of Report and Period Covered: Final Report 9/29/78 - 9/29/79
12. Sponsoring Agency Name and Address: Environmental Protection Agency Cincinnati, Ohio 45268		14. Sponsoring Agency Code: EPA-MAP

15. Supplementary Notes

16. Abstract

The design and development of a machine to measure tire energy dissipation over transient driving cycles is described. The main feature of the machine is that two tires are loaded against each other across a steel belt which runs on 762-mm diameter steel drums. One of the wheels is driven to follow a transient driving cycle representative of typical passenger car use; the other wheel is allowed to roll freely. Energy dissipation in the driving tire is measured by subtracting the energy leaving the tire from the energy entering the tire. An error, ascribed to small deformations of the belt in the tire contact area, was found in the tire energy measurement. This error is a function of the construction of the tires installed on the machine. A number of modifications to the machine and the test procedures are suggested to improve the accuracy of the energy dissipation measurements. Typical energy dissipation measurements for C-14 tires are presented.

17. Key Words	18. Distribution Statement
automobile tires, energy dissipation	Available from: National Technical Information Service U.S. Department of Commerce Springfield, VA 22161

19. Security Classif. (of this report)	20. Security Classif. (of this page)	21. No. of Pages	22. Price
		83	

Form DOT F 1700.7 (8-69)

PTI 8212

TIRE ENERGY DISSIPATION DETERMINATION

Final Report

Submitted to

United States Environmental Protection Agency

by

Gordon F. Hayhoe
Assistant Professor of Mechanical Engineering

The Pennsylvania Transportation Institute
The Pennsylvania State University
University Park, Pennsylvania 16802

July 1982

TABLE OF CONTENTS

		Page
1.	INTRODUCTION	1
2.	SUMMARY OF MACHINE DESIGN AND OPERATION	3
	2.1 Machine Frame	3
	2.2 Roadway	3
	2.3 Wheel Assemblies	6
	2.4 Wheel Loading Mechanism	6
	2.5 Drive System	6
	2.6 Instrumentation System	8
	2.7 Data Collection System	11
3.	SYSTEM DEVELOPMENT	13
	3.1 Motor Drive	13
	3.2 System Timing	15
	3.3 Low Speed Operation	15
	3.4 Transducer Temperature Drift	15
	3.5 Flexible Coupling	18
	3.6 System Calibration	18
	3.7 Energy Measurements	33
4.	SUGGESTED MODIFICATIONS	38
	4.1 Individual Force Calibration	38
	4.2 Corrected Force Calibration	38
	4.3 Indirect Measurement of Roadway Losses	38
	4.4 Equal Torque Drive	39
	4.5 Free-Rolling Resistance Force Measurements	40
5.	CONCLUSIONS	41
REFERENCES		42
APPENDIX A.	MACHINE COMPONENTS	43
APPENDIX B.	MOVEMENT OF THE CENTER OF TIRE CONTACT PRESSURE WITH DRIVING AND BRAKING FORCES	62

LIST OF FIGURES

Figure		Page
1	Schematic of Tire Test Machine for Measuring Rolling Resistance Losses	4
2	Two Views of the Test Machine Showing the Major Mechanical Details	5
3	Layout of the Motor Speed Command Voltage Generator Circuit	7
4	Block Diagram of the Signal Conditioning Circuit	9
5	Basic Layout of the Data Counter Interface in the Data Acquisition System	12
6	Motor Speed Response Over the First Two Minutes of the EPA Urban Cycle (Transient Segment)	14
7	Force Transducer Temperature Drift Test Results	17
8	Results of Force Transducer Calibration, Set 1	20
9	Results of Force Transducer Calibration, Set 2	21
10	Results of Force Transducer Calibration, Set 3	22
11	Results of Force Transducer Calibration, Additional Radial Tire Tests in Set 3	24
12	Results of Force Transducer Calibration, Additional Belted Tire Tests in Set 3	25
13	Simplified Schematic of the Belt/Tire System	29
14	Energy Dissipated in the Driving Tire Over the Transient Segment of the EPA Urban Cycle	31
15	Constant Speed Rolling Resistance Test Results	36
A-1	Roadway Drum Dimensions	45
A-2	Inertial Load Drive Speed Reducer	46
A-3	Flexible Coupling (Series 52)	47
A-4	Flexible Coupling Stiffness Data	48
A-5	Torque Transducer	50
A-6	Lower Down Location and Loading Mechanisms	51

LIST OF FIGURES

Figure		Page
A-7	Tire Loading Mechanism - Top View	52
A-8	AD581 Precision Voltage Reference	53
A-9	AD521 Instrumentation Amplifier	54
A-10	AD517 Precision Operational Amplifier	55
A-11	AD534 Precision Analog Multiplier	56
A-12	AD537 Voltage To Frequency Converter	57
A-13	ICL7601 (now AM 7601) Commutating Auto-Zero Amplifier	59
A-14	Analog Devices Model 289 Precision Hybrid Isolation Amplifier	60
A-15	Interrupt Line Buffer Circuit	61
B-1	Force and Moment System Acting on the Tire	64
B-2	Longitudinal Force Characteristics	73
B-3	Rolling Moment	74
B-4	Rolling Resistance Moment for the Bias Belted H78-15 Tire versus Longitudinal Force at	75
B-5	Rolling Resistance Moment M_y versus Longitudinal Force F_x for a Steel-belted GR78-15 Radial Tire	77

LIST OF TABLES

Table		Page
1	Variables Allocated to Data Channels	10
2	Force Transducer Temperature Drift Test Results	16
3	Force and torque Transducer Zero Offset Measurements Corresponding to the Test Results in Figure 14	32
4	Energy Flow During the Transient Segment of the EPA Urban Cycle	34
5	Peformance of Bias and Belted Tires Relative to the Raidal Tire for Different Test Measurements	37
A-1	Tire and Rim Association Passenger Tire Load Ratings With Corresponding Inertia Loads Required to Simulate One Half of a Car on the Machine	44
B-1	Measured Tire Data	72

1. INTRODUCTION

The objectives of the project were:

1. To acquire and construct test equipment to simulate a vehicle traveling over transient driving cycles representative of typical consumer passenger vehicle usage for the purpose of obtaining information on the energy dissipated by the tires of a vehicle over such cycles. The equipment is to be capable of measuring total energy dissipated over the cycles with good precision so that tires of different make and type can readily be distinguished and their relative effect on vehicle fuel consumption estimated.

2. To obtain energy dissipation information from a sample of 100 tires when these tires are operated over the EPA urban cycle and the EPA highway fuel economy cycle. The results are to be analyzed with respect to all of the tire parameters varied in the sample.

In response to the first objective, a test machine was designed and built. The main feature of the machine is that two tires are loaded against each other across a steel belt. One of the wheels is driven to follow the required driving cycle, and the other wheel is allowed to roll freely. The energy dissipated in the driving tire is measured by subtracting the energy leaving the tire from the energy entering the tire.

During development of the machine it was found that the measurement of tire force was not sufficiently accurate to meet the specified error in energy loss determination. After the presence of an unacceptably large error had been established, the remaining project resources were expended in identifying and attempting to eliminate the source of the error. The second project objective of measuring the energy loss of a sample of 100 tires, therefore, was not completed. The cause of the error, and its significance in the tire energy determination, is discussed briefly below and in detail in the body of the report.

The maximum force transmitted by the driving tire to the belt during the EPA cycles is approximately one third of the vertical load. Lateral forces on the belt arise only from steer angle misalignment in the machine, tire properties such as ply-steer, and manufacturing nonuniformities. These forces are small compared to the forces normally generated on a tire test machine, and it was estimated during the design stages that belt deformation would have a relatively small effect on machine accuracy.

The most critical element in the energy dissipation measurement procedure is the accurate determination of drive torque and driving wheel force since these two quantities, multiplied by wheel speed and roadway speed respectively, are subtracted to find energy loss. Each transducer must have a full-scale range exceeding the maximum value of the measured variable during the driving cycle. But at maximum load the absorbed energy is only a small fraction of the transmitted energy (approximately 5 percent). At minimum load the absorbed and transmitted energies are approximately equal, but the transducer accuracies are still determined by the full-scale ranges.

Errors in the force and torque measurements due to transducer and signal conditioning nonlinearities and to calibration errors were not expected to be significant in this application because the errors would essentially be constant from one test to another. This follows from the fact that the energy required to drive the machine with different tires installed differs only by the difference in the energy dissipated by the tires, which is small compared to the total energy. The accuracy of relative tire performance measurements would therefore tend to be better than indicated by the errors in the absolute values of the measurements. The machine effectively operates over only a small part of its operating range about a point determined by the driving cycle. On the other hand, long-term and temperature drift effects were expected to present considerable problems because the consequent errors are not constant from test to test and are cumulative over a complete cycle.

During development of the machine, temperature drift in the force transducers was found to be excessive. This can be remedied by installing more suitable transducers. The most serious problem encountered was that the wheel force measurements were found to contain an error which is independent of the transducer and the signal conditioning circuits. The error is probably caused by small amounts of belt deformation and is a function of the construction characteristics of the tire installed on the machine. Unacceptably large errors are thus introduced into the tire energy dissipation measurements, which cannot be eliminated with the machine and test procedures as they are presently used. Possible modifications which may be made to the machine to eliminate or reduce the error are discussed in Section 4.

2. SUMMARY OF MACHINE DESIGN AND OPERATION

The machine is a flat belt design (see Figure 1) with two tires loaded against each other across the belt. One of the tires is driven by a DC electric motor while the other is free rolling. The inertia of the belt drums is augmented by a flywheel whose inertia can be adjusted to correspond to the equivalent inertia of the tire load. The DC motor is programmed to follow the speed history of the desired driving cycle. Strain gauge transducers measure the necessary tire forces and drive torque. Analog integrated circuit multipliers directly measure the power flowing into and out of the system, while a small microcomputer system is used to collect, reduce, and store the data.

The major mechanical components of the machine, shown in Figure 2, consist of: (a) main frame, (b) an endless steel-belt roadway running on crowned steel conveyor-belt drums, (c) wheel axle and force transducer assemblies mounted on ball bushing pillow blocks, (d) a wheel-loading mechanism, and (e) a DC electric motor and drive. Instrumentation signal-conditioning components are contained in a number of shielded metal boxes located as close as possible to their associated transducers. Data transmission is via voltage to frequency (V/F) converters to the remotely located data collection system. Data integrity is thus preserved in the presence of the high electrical noise generated by the motor and chopper controller.

Each of the major subsystems is briefly described below. Where appropriate, a more detailed description is given in Appendix A, together with manufacturers' specifications for key components.

2.1 Machine Frame

The two roadway drums are mounted on a framework constructed from 100 mm by 100 mm square steel tubing of 6.4 mm wall thickness. The two side frames are of welded and bolted construction, joined by bolted cross pieces. Lateral stiffening members are bolted to the side frames at the drum mounting points. The complete assembly is bolted rigidly to the floor.

2.2 Roadway

The roadway consists of an 0.8-mm thick by 400-mm wide butt-welded steel belt running on two welded steel conveyor belt drums, 762 mm in diameter by 457 mm wide. To maintain lateral belt stiffness at as high a value as possible, belt tension is set at the maximum value consistent with good fatigue life (see Reference 1). Because of the high belt load, the drums were manufactured with thicker than standard rims. The rims were then machined and the drums dynamically balanced.

The upper drum is mounted directly to the frame and turns in ball-bearing pillow blocks. The lower drum turns in ball-bearing flanged units. The flanges are guided vertically by watts linkages on each side of the frame (see Figure A-6). Lateral constraint is provided by two radius arms located on one side of the frame. The drum bearings have low-friction mechanical seals.

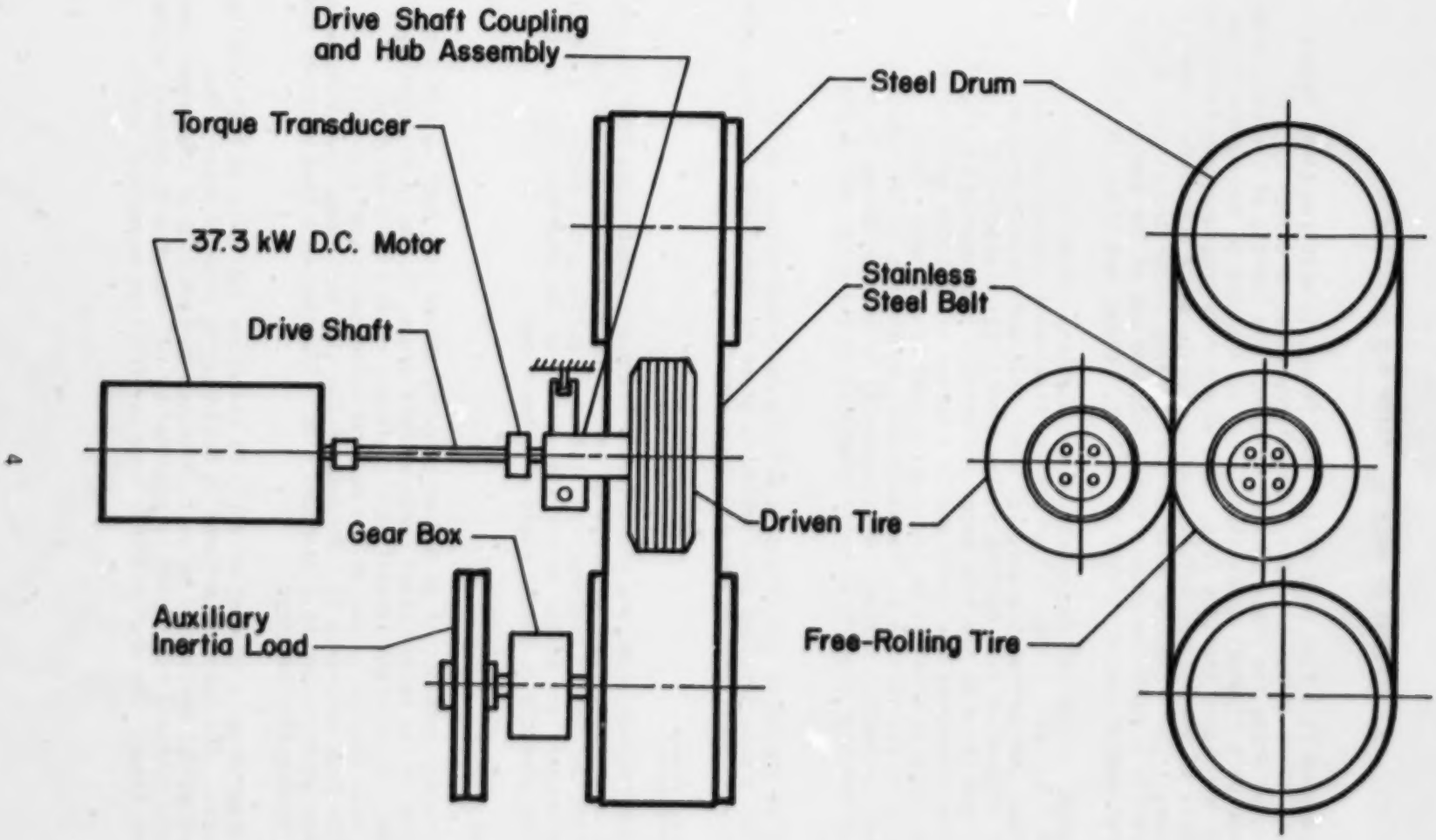

Figure 1. Schematic of Tire Test Machine for Measuring Rolling Resistance Losses

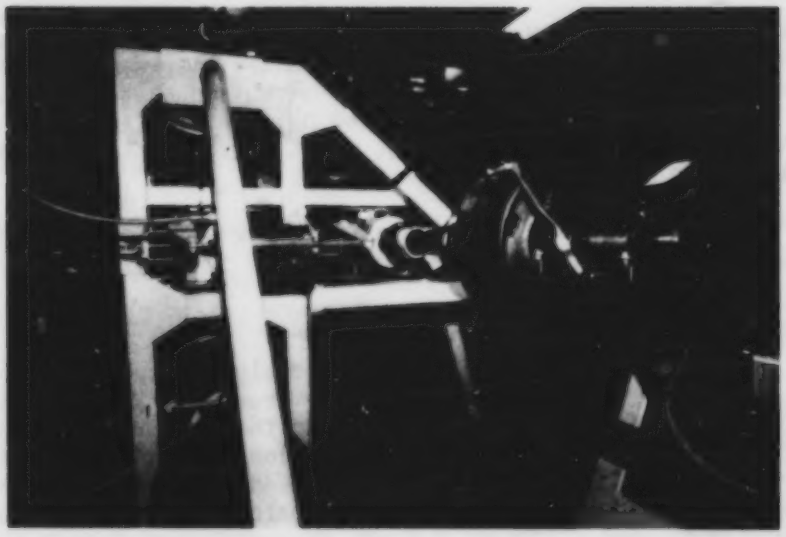

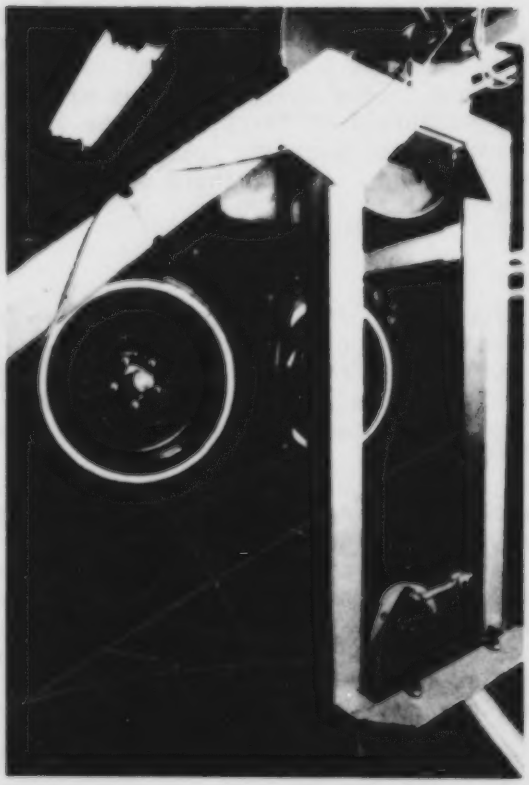

Figure 2. Two Views of the Test Machine Showing the Major Mechanical Details

A belt preload of 44 kN (22 kN per side) is applied to the lower drum through the bearing flanges and a stack of belleville washers. The belleville washers are initially compressed a predetermined amount to apply the (nominal) preload. The deflection of (force applied by) the washers on one side is then adjusted to give correct belt tracking. Belt replacement is accomplished by removing a section of one of the side frames.

The roadway has a maximum design surface speed of 96 km/h and will accommodate tires of up to 760 mm in diameter.

2.3 Wheel Assemblies:

Each wheel is mounted on a hub/axle assembly which, in turn, is fixed to a two-axis (vertical and longitudinal) force transducer. To reduce friction as much as possible, seals were not fitted to the axle bearings, and light machine oil was used for lubrication. The unloaded bearing friction torque was measured at approximately 0.12 N m. The additional bearing friction torque due to loaded rolling losses was estimated by assuming a coefficient of friction of 0.002. For a load of 4.5 kN, the additional torque is thus approximately 0.25 N m.

2.4 Wheel Loading Mechanism

The wheel/axle assemblies are mounted on low-friction, recirculating, ball-bushing, pillow block linear bearings so that the axles move on a common line which is normal to the belt surface. A rolling diaphragm pneumatic cyclinder applies the load to the axle assemblies via two rocking beams (see Figure A-7). With the exception of friction in the linear bearings and beam bearings, both tires experience the same load. The roadway drums are mounted vertically, one above the other, to eliminate dead weight loading on the tires. The maximum design load is 6 700 N.

2.5 Drive System

The drive system consists of a 37.3 kW DC electric motor, an SCR chopper motor controller, and a driving cycle generator. Drive from the motor to the wheel is through an automobile drive shaft, a torque transducer, and a metallic flexible coupling. The function of the flexible coupling is to isolate the wheel force transducer from forces generated by drive shaft vibration and misalignment.

The complete roadway/drive system operates as a feedback control system, with the error signal derived from a tachometer generator roadway speed signal and a speed command voltage. A circuit was built to generate the required motor control command voltage from information stored digitally in erasable, programmable, read only memories (EPROM). The information in the memories is read sequentially once per second and passed to a 12 bit digital/analog converter. The resulting step-change driving cycle speed history is then shaped to a ramped history and passed to the motor drive error amplifier. The flow chart shown in Figure 3 illustrates the operation of the driving cycle generator circuit. The drive system can also be switched to a manual control mode, in which a ten-turn potentiometer is used to adjust motor speed.

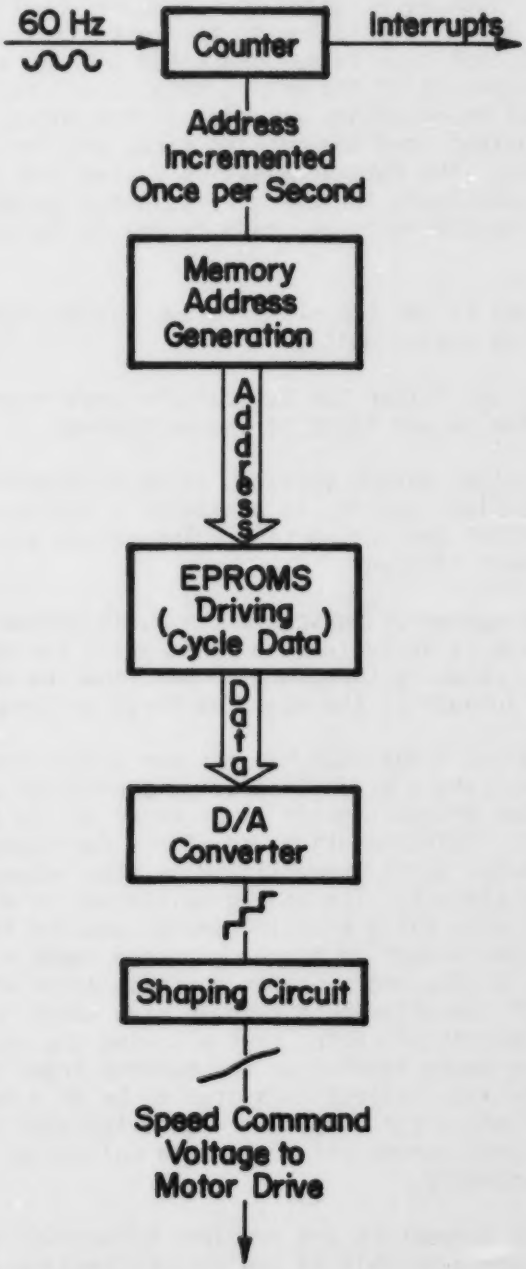

Figure 3. Layout of the Motor Speed Command Voltage Generator Circuit

2.6 Instrumentation System

The primary elements in the instrumentation system are force and torque strain gauge transducers, which measure vertical and longitudinal tire forces and drive torque. Tachometer generators measure wheel speed and roadway drum speed. Since the energy dissipated in the test tires is required over a driving cycle with continuously varying speed and for a tire transmitting torque, simple processing of the analog data is not sufficient. In the scheme adopted, individual measurements are made of the energy input to the driving tire, the energy output from the driving tire, and the energy input to the freely rolling tire. The data acquisition system then scales the resulting measurements and calculates the energy dissipated in the tires. The individual energy measurements are made by the following method (see also Figure 4):

(a) Amplify and filter the strain gauge bridge signal and pass to one input of an analog multiplier.

(b) Attenuate and filter the appropriate tachometer generator signal and pass to the second input of the multiplier.

(c) The multiplier output voltage, which is proportional to power (force or torque times speed), is passed to a voltage/frequency (V/F) converter for conversion to a pulse stream whose frequency is proportional to power.

(d) Count the number of pulses in the pulse stream over a given period of time. This is equivalent to integrating the multiplier output, and the count value is therefore proportional to the work done (energy input or output) by the measured force or torque.

Each strain gauge transducer has its own signal conditioning system which includes a low temperature drift, isolated, excitation power supply. Amplification of the bridge signals is by means of low temperature drift, integrated circuit, instrumentation amplifiers for rejection of common mode signals. An ultra-low drift preamplifier is also incorporated in the longitudinal force circuit. The analog multiplier is a high quality integrated circuit with fully floating inputs and the following major specifications: feedthrough on force or torque input = ± 0.003%; feedthrough on speed input = ± 0.05%; and transfer function error versus temperature = 0.008%/°C. The V/F converter outputs have high noise immunity and can be passed over long lengths of cable, thus allowing the analog signal conditioning system to be located on the machine frame close to the transducer, and the data collection system to be at a convenient, remote, location. The V/F converter outputs are also isolated from the analog system ground, and the signal conditioning and data collection systems can therefore be operated independently.

Additional V/F converters are provided to monitor each transducer output. Twelve data lines are available in the data collection system (a list of the monitored variables is given in Table 1). Multiplexing a number of V/F converters on the same data line is relatively straightforward, and additional low-frequency signals (such as temperature and pressure) could be sampled without changes being made to the data collection system hardware.

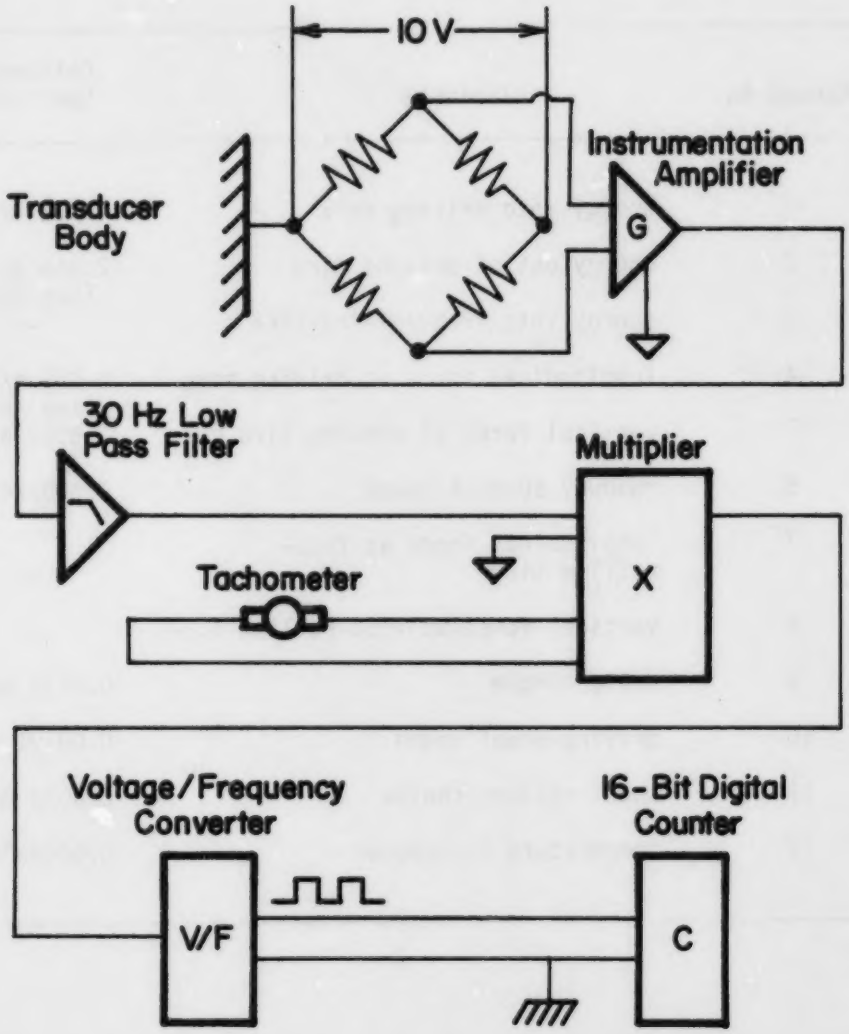

Figure 4. Block Diagram of the Signal Conditioning Circuit

Table 1. Variables Allocated to Data Channels

Channel No.	Variable	Calibration Coefficient
1	energy into driving tire	1.222 J/count
2	energy out of driving tire	2.464 J/count (see text)
3	energy into free-rolling tire	--
4	longitudinal force at driving tire	0.085 N/count (see text)
5	vertical force at driving tire	0.0952 N/count
6	roadway surface speed	0.000574 m/s/count
7	longitudinal force at free-rolling tire	--
8	vertical force at free-rolling tire	--
9	drive torque	0.0119 Nm/count
10	driving-wheel speed	0.00191 rad/s/count
11	wheel rolling radius	0.0032 mm/count
12	temperature transducer	0.00583°C/count

2.7 Data Collection System

The data collection and reduction system is based on an AIM 65 microcomputer development system. The system is shown in block diagram form in Figure 5 and has the following major features:

(a) 6502 processor
(b) assembler in ROM
(c) 8 k bytes BASIC interpreter in ROM
(d) 36 k bytes RAM
(e) two magnetic tape cassette drives
(f) four programmable digital counter chips, each containing three 16 bit counters.

The functions of the system are to count the number of pulses sent by the instrumentation V/F converters during each one-second increment of the driving cycle, read the count values and convert them to engineering units, calculate the tire energy dissipation, and store the reduced data.

The digital counter interface requires only decoding of the computer address lines and access to the data lines. Access to the counters is then by memory READ/WRITE instructions, and rapid reading of the counters is possible. The program for reading the counters is written in assembly language and the read cycle is initiated by a once per second interrupt from the driving cycle speed command generator circuit. The counters are read in groups of four, and each counter is inhibited for 10 μs while the counter contents are latched. Full-scale output from the V/F converters is 50 kHz (20 μs pulse width), so a maximum of one pulse is missed during the latching operation. To read all twelve counters and store the data values in temporary storage takes a total of 250 μs. When the read cycle has been completed, control is passed to a BASIC program which converts the stored values to engineering units by using calibration data supplied prior to the test run. After the tire energy dissipation has been calculated, over the second for which the data are valid, all data values are stored in memory locations corresponding to the point in the driving cycle during which the data were generated. (BASIC calculations are done in 10-digit floating point arithmetic, although only 16 bits of the resulting numbers are stored.) After the data reduction and storage routine is completed, control is passed back to the assembly language routine which is ready to read the counter values on the next interrupt.

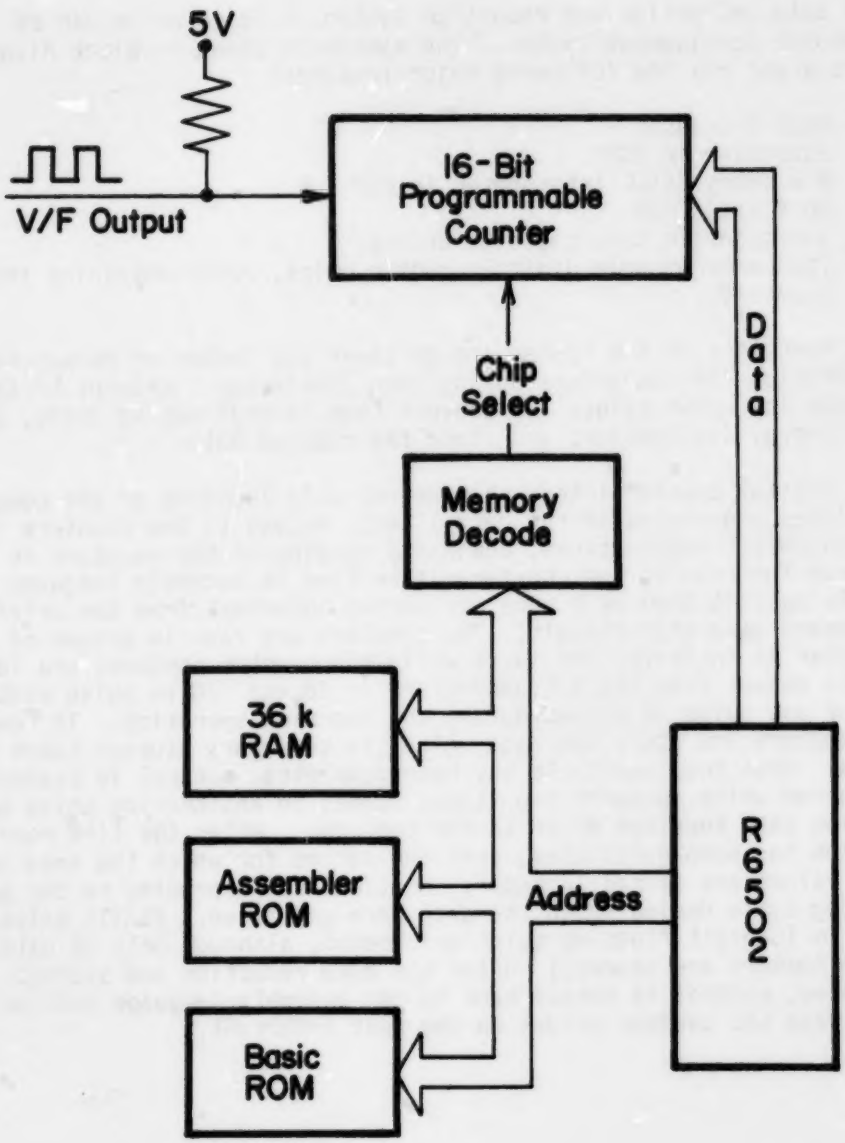

Figure 5. Basic Layout of the Data Counter Interface in the Data Acquisition System

3. SYSTEM DEVELOPMENT

A number of problems were encountered in developing the machine. All of the problems except two were resolved and corrected satisfactorily. The first unresolved problem was the excessive temperature drift in the force transducers, which could probably be remedied by using different transducers. The second was probably due to the effects of deformation of the belt in the area of the tire contact patches. This was first noticed during calibration of the drive wheel force transducer, when slightly different operating conditions gave different calibration coefficients. If the diagnosis of the problem is correct, substantial modification to the machine will be required. The development of the machine proceeded in a number of well-defined stages, each of which is described separately below.

3.1 Motor Drive

The function of the motor drive system is to control the speed of the drive wheel so that the EPA urban and highway cycles are executed by the machine accurately and repeatably. As delivered, the motor drive was set up for proportional plus integral control, with an excessively long time constant when the wheels and drums were driven. This tended to smooth out the speed fluctuations in the EPA cycles. Simply increasing the system gain was not effective, because the high inertia and low damping inherent in the machine did not allow the response time to be decreased sufficiently without introducing underdamped behavior. Modifications to the controller included changing the proportional and integral feedback coefficients and adding a positive feedback derivative term to increase the natural frequency. For the latter modification, the motor tachometer signal is differentiated and the resulting voltage added to the speed command voltage signal.

Figure 6 shows roadway speed over the first two minutes of the EPA urban cycle (transient segment) with the drive control system in its final configuration. Plots are shown for the drive wheel unloaded and freely turning, and for the wheels loaded and driving the roadway with full inertial load. The plot of the unloaded run is an accurate reproduction of the specified cycle, while the plot for the loaded run shows some smoothing of the high frequency speed fluctuations. The cycle is, however, well within the specified limits for emissions tests and, for a given inertial load, was found to be highly repeatable. Further improvement in the response time of the system could probably be achieved, but this would entail custom modification of the controller circuitry by the drive manufacturer and was not deemed necessary. It should be noted that the control system should be well overdamped to ensure that high frequency torque fluctuations do not occur. Accurate tracking of the desired speed cycle does not necessarily mean that the applied torque is uniform or repeatable over short periods of the cycle.

Although most of the machine development tests were run at relatively low belt speeds, high-speed operation was checked by running the machine at constant speed for periods of 30 minutes. At the end of each 30 minute period the speed was increased by 10 km/h until the maximum design speed was reached. The test was completed satisfactorily.

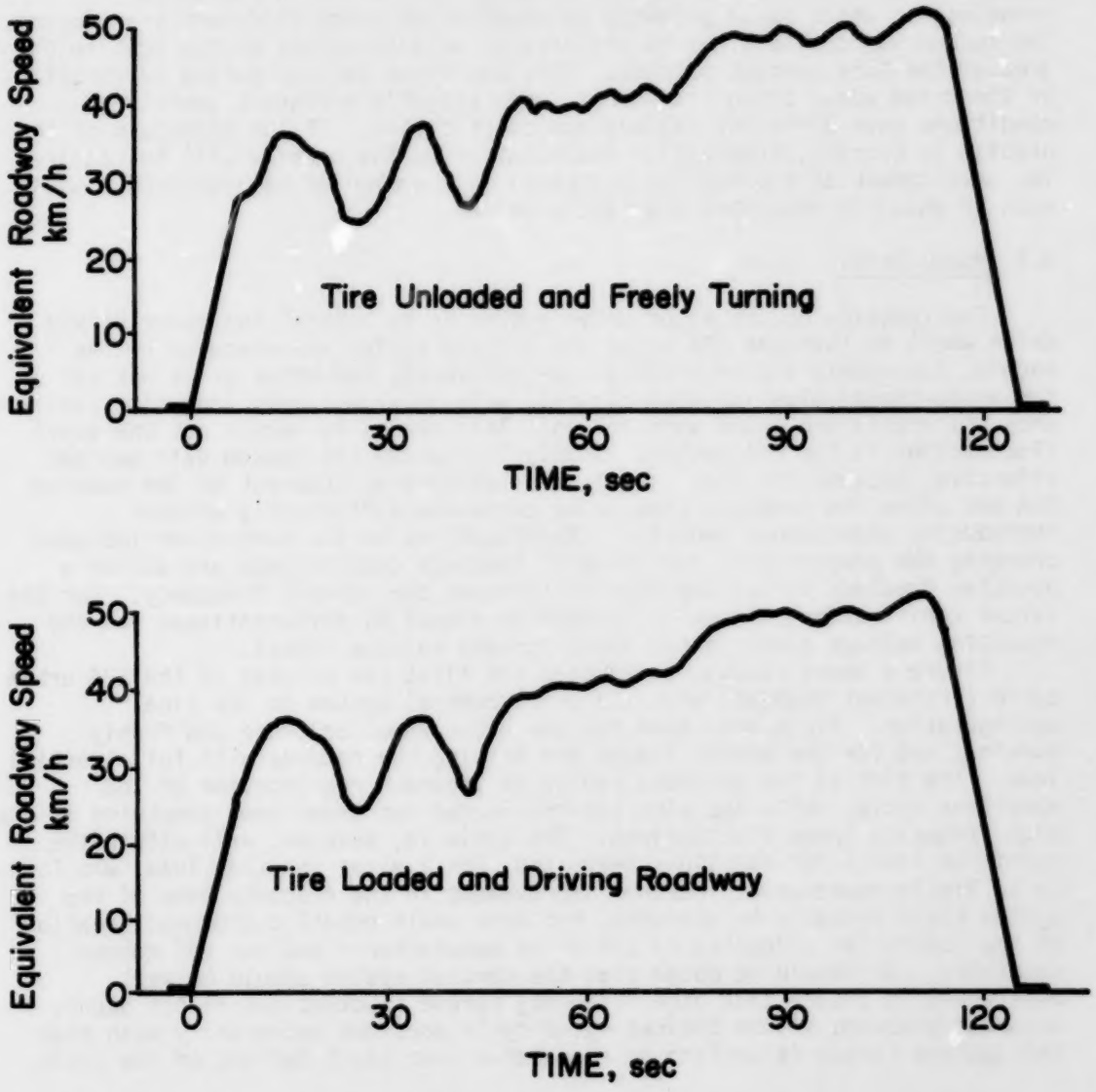

Figure 6. Motor Speed Response Over the First Two Minutes of the EPA Urban Cycle (Transient Segment). CR78-14 tire unloaded (freely rolling) and at 3,300 N vertical load (driving roadway)

3.2 System Timing

The EPA cycles are described by a sequence of numbers (velocity) spaced at one-second intervals. Overall system timing is therefore derived from a 1-Hz clock, with motor speed command voltage incremented and a data collection cycle initiated by the same once per second signal. Since the data collection process consists of integrating the analog signals over each one-second interval, the 60-Hz mains frequency in the analog signals can be rejected by dividing the mains frequency to 1 Hz to give the system timing signal. This scheme was incorporated in the first design, but, although utility companies are required to maintain a very accurate 24-hour mains cycle count, significant short-term variations were found in the mains frequency. Bursts of noise on the line further affected measurement accuracy, so the scheme was abandoned in favor of using a 1 Hz square wave derived from the microcomputer crystal controlled clock. The improvement in measurement accuracy given by the stable clock far exceeded the errors caused by mains noise pickup.

A further problem was that switching transients from the motor controller were sometimes large enough to interrupt the microcomputer and initiate spurious data collection cycles. Various isolation techniques were tried, and the somewhat crude method of low-pass filtering the interrupt lines was found to be most effective (see Appendix A). The time delay caused by the filters is unimportant because relative (cycle to cycle) accuracy is required rather than absolute timing accuracy.

3.3 Low Speed Operation

An inherent feature of DC chopper controllers is that they give poor speed control at very low motor speeds. During the portions of the driving cycles where zero speed is specified, there was usually some residual wheel rotation and oscillation of drive torque. To eliminate this as a possible source of error in the overall energy measurement, the data reduction program was modified to ignore all incoming data, and to set energy dissipated in the tires to zero when the speed command signal is zero.

3.4 Transducer Temperature Drift

As discussed previously, extremely low offset drift of the force, torque, and speed measurements is necessary for the accurate measurement of tire energy dissipation. During the early tests it was noticed that the drive wheel force transducer exhibited unacceptably high drift. This was tentatively ascribed to drift in the instrumentation amplifier and an ultra-low drift (Datel/Intersil AM-7601) preamplifier was placed between the transducer output and the instrumentation amplifier. The preamplifier was set at a gain of 1,000 and the instrumentation amplifier gain reset at approximately 2.5. The overall drift performance of the force measurement was not materially affected by the modification, so the tranducer itself was checked. An integrated circuit temperature transducer (AD 590) was glued to the body of the force transducer, and the complete assembly was wrapped with insulating material. The force measurement and the force transducer temperature were then monitored over a period of two days. Table 2 and Figure 7 show the results of the test. A very strong correlation is evident between force measurement drift and transducer temperature, with approximately 1.5 N hysteresis between increasing and decreasing temperatures. The drift

Table 2. Force Transducer Temperature Drift Test Results.

Date	Time	Ambient Temperature °C	Instrumentation Box Temperature °C	Change in Temperature of Transducer °C	Change in Force Measurement N
7/29	2:10 pm	24.7		0.43	3.34
	2:55 pm	24.9		0.54	4.00
	3:30 pm	25.6		0.66	4.67
	3:55 pm	25.8		0.78	5.30
	4:15 pm	25.8		0.86	5.87
	5:00 pm	26.1		1.03	6.85
	5:05 pm	26.1		1.07	7.08
	5:15 pm	26.1		1.12	7.30
	5:40 pm	26.1		1.21	7.88
	6:10 pm	26.3		1.31	8.54
	6:30 pm	26.3	34.3	1.39	8.19
	6:40 pm	25.8	34.2	1.41	8.32
	7:50 pm	25.2	33.6	1.46	7.88
	8:25 pm	25.1	33.4	1.45	7.88
	8:55 pm	24.9	33.3	1.44	7.74
	10:55 pm	-	-	1.35	6.99
	11:30 pm	-	-	1.13	5.87
7/30	1:30 am	24.3	32.4	0.99	5.07
	12:25 pm	23.8	31.9	0.00	0.00
	1:45 pm	-	-	0.16	1.02
	4:30 pm	24.5	-	0.55	3.43

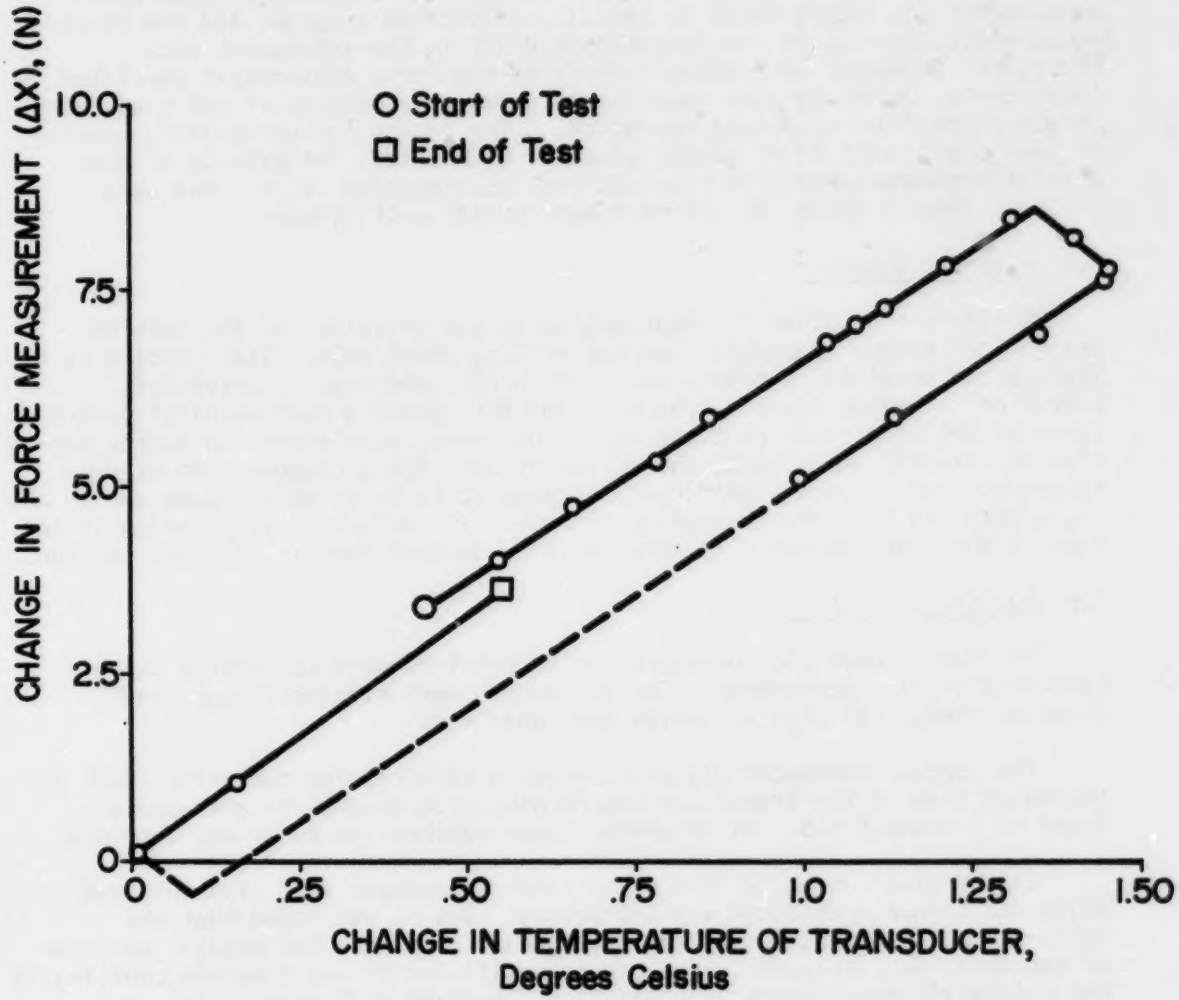

Figure 7. Force Transducer Temperature Drift Test Results

coefficient translates to approximately 0.15 percent of full scale per degree C, somewhat high for a precision transducer. Other tests, with the preamplifier inputs grounded, indicated that the drift of the signal conditioning instrumentation was approximately an order of magnitude lower than the force transducer drift.

Because of the good correlation obtained, the transducer temperature measurement was incorporated in the data collection program, and the force measurement compensated for temperature drift in the subsequent data reduction. However, unacceptable drift of the force measurement persisted in later tests, which may have been due to asymmetric heating of the transducer strain gauges during machine operation. (The transducer essentially consists of four posts, with eight gauges glued to each post.) The effects of this problem are demonstrated in the test results presented later. The only solution appears to be the use of a more suitable transducer.

3.5 Flexible Coupling

A flexible coupling is incorporated in the driveline of the machine between the torque transducer and the driving wheel axle. Its function is to isolate the wheel-force transducer from forces generated by driveshaft vibration and misalignment. The coupling introduces a nonsinusoidal periodic force at the wheel axle of three cycles per wheel revolution and approximately 12.5 N peak-peak amplitude. The effect of this force component on overall system accuracy is not significant, because it tends to be averaged out by the integration in the data collection process. Its effect on calibration of the force transducer, however, is more serious, as described in the next section.

3.6 System Calibration

The motor speed and roadway speed tachometers were calibrated using a hand-held digital tachometer. The procedures were straightforward and accurate linear calibration curves were obtained.

The torque transducer was calibrated by constraining the drive shaft on the motor side of the transducer and hanging dead weights on a torque arm fixed to the wheel hub. An accurate linear calibration curve was obtained.

Calibration curves for the wheel force transducer were also obtained while the torque transducer was calibrated. But it was found that the calibration constant given by the procedure varied with the angular position of the wheel hub, presumably because the stiffness of the flexible coupling in the driveshaft also varies with position. A means of "dynamically" calibrating the force transducer was therefore sought. The most satisfactory arrangment would be to mount a dynamometer (fluid or electrical coupling) on the wheel hub and measure the moment arm force required to constrain the dynamometer body while the wheel is turning. Averaging the moment arm force and force transducer output over a number of hub revolutions and for a number of dynamometer settings would give the required calibration relationship. Suitable equipment was not available though, and an alternative procedure was tried in which tire rolling resistance force is measured. The procedure consisted of the following steps:

1. Mount two nominally identical tires on the machine.

2. Run the machine at light load (approximately 125 N) and constant speed, and measure input torque and drive tire force transducer output averaged over 60 seconds.

3. Run the machine at rated load for the tires and constant speed, and measure input torque and drive tire force transducer output averaged over 60 seconds.

4. Calculate rolling resistance force as measured by the torque transducer and calculate the change in force transducer output (X_R) from step 1 to step 2, i.e.:

$$F_R = \frac{T_2}{2R_2} - \frac{T_1}{2R_1}$$

$$X_R = X_2 - X_1$$

where

T_1, T_2 = torque measurement for steps 1 and 2 respectively.

R_1, R_2 = tire rolling radius for steps 1 and 2 respectively.

X_1, X_2 = force transducer output for steps 1 and 2 respectively

T_1/R_1 gives the force at the roadway surface required to drive the roadway at constant speed, plus the light load rolling resistance force of both tires.

T_2/R_2 gives the same forces except that rolling resistance force is greatly increased.

The factor of 1/2 gives the rolling resistance force of one tire assuming that the forces generated by both tires are equal.

5. Change the tire pressures and repeat the procedure.

6. Plot F_R against X_R and find the slope of the curve.

The calibration procedure was run with three different tire sets (bias, bias-belted, and radial ply construction). Significantly different calibration coefficients were obtained with each tire. Since accurate calibration of the force transducer is essential to correct machine operation, further tests were run in an attempt to identify the apparent error. Figures 8 through 12 show the results of the three series of tests. The results marked "reversed" were obtained with the driving and free rolling tires interchanged.

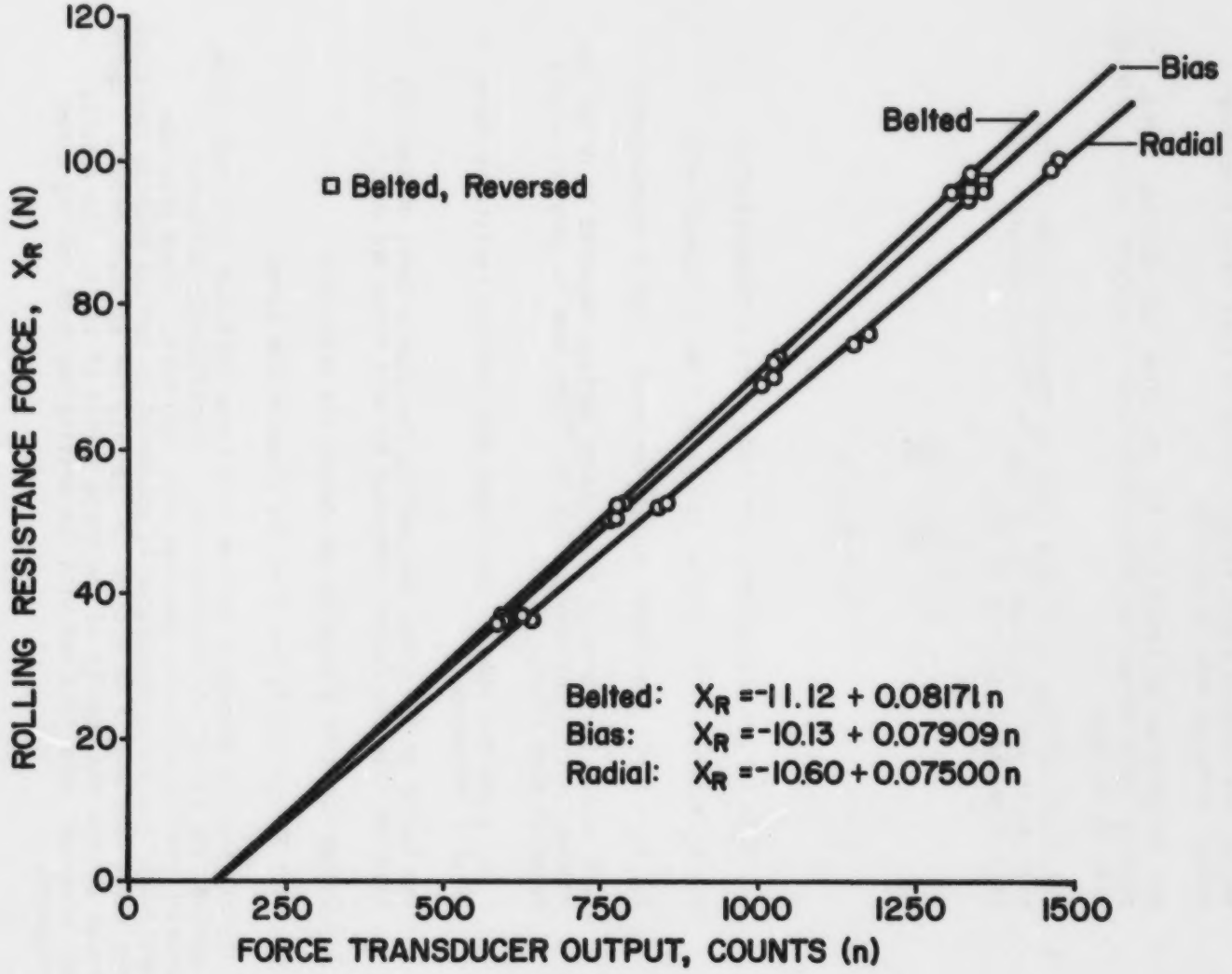

Figure 8. Results of Force Transducer Calibration, Set 1

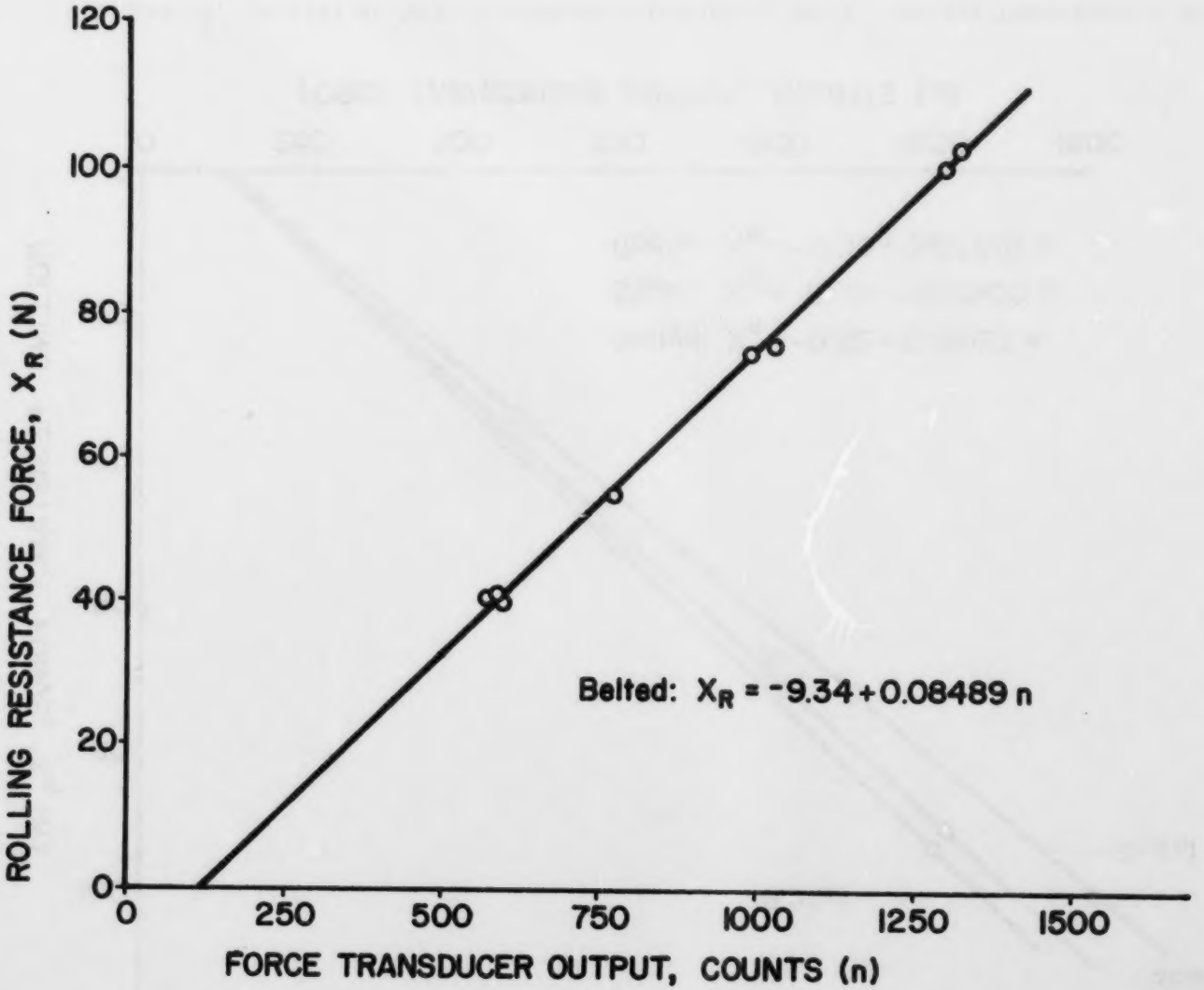

Figure 9. Results of Force Transducer Calibration, Set 2. Ambient Temperature = 22.2°C.

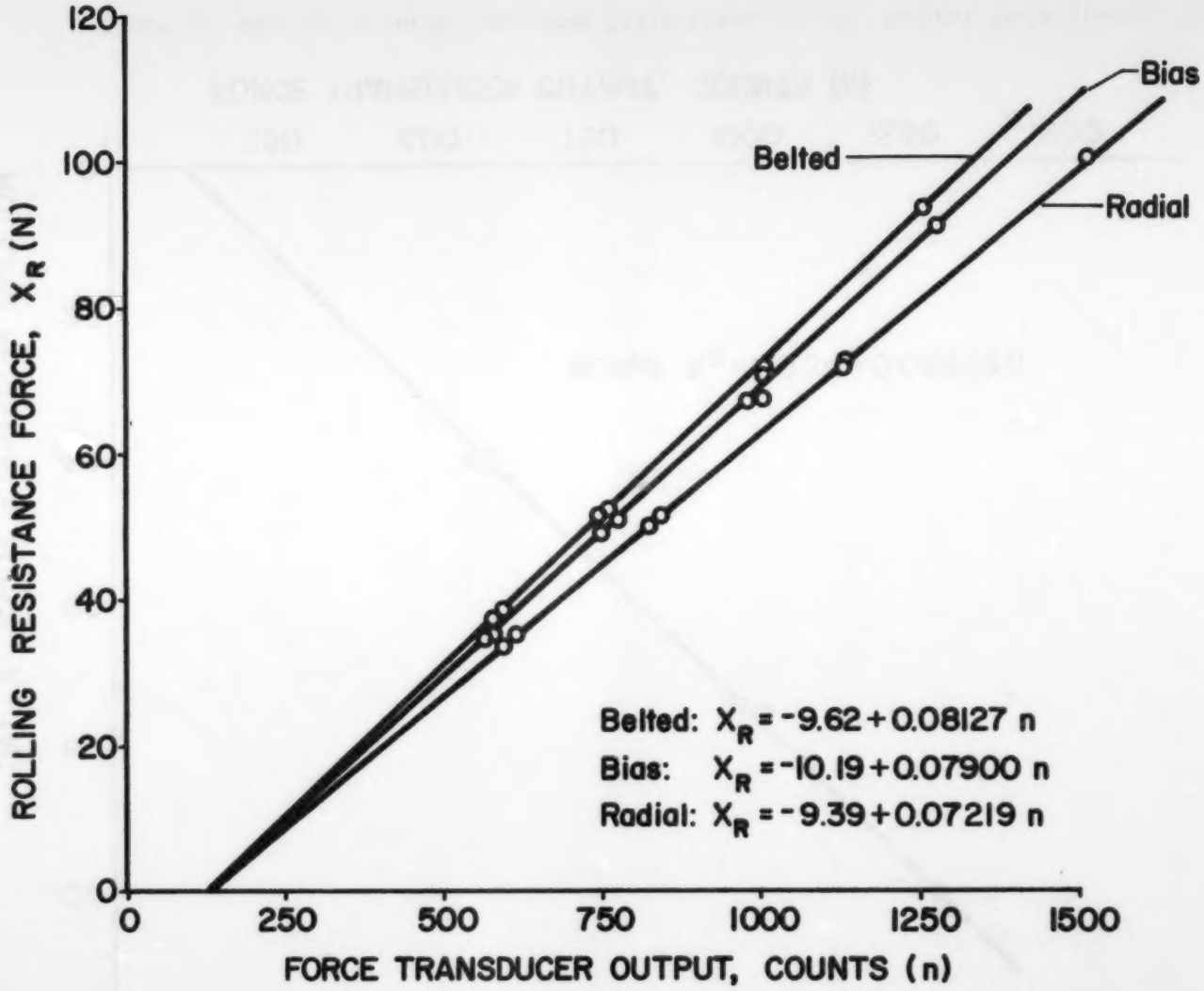

Figure 10. Results of Force Transducer Calibration, Set 3. Ambient Temperature = 26.7°C.

In deriving the results of the calibrations, it was assumed that the energy loss is the same in the free rolling tire as it is in the driving tire. A more accurate statement may be that the force entering the free rolling tire is the same as the (apparent) force lost in the driving tire [(torque in) equals (twice the rolling resistance force of the free rolling tire plus the parasitic belt and drum force) times (the rolling radius of the driving tire)]. There are a number of possible causes of asymmetric energy loss.

(1) Although the tire pairs were purchased at the same time and from the same supplier, the individual tires in a pair may have slightly different characteristics.

(2) The energy loss in the driving tire may be slightly different from that in the free rolling tire because it is transmitting torque. The ratio of energy loss in a tire pair also may be different for different tire constructions.

(3) The two wheel axles are not aligned accurately enough and the two tires are running at significantly different slip angles.

Figure 11 (radial, normal and reversed) indicates that slip angle effects and nonuniform tire characteristics in the radials were not signficiantly large. Figure 12, however, indicates a difference in the characteristics of the two belted tires, although the effect on the results was not large enough to make the reversed belted curve coincide with the radial curve.

The second explanation is more difficult to assess because its effects cannot be isolated by reconfiguring the machine or the tires. It is probable that the effect is not large enough to explain the large difference between the curves obtained for the belted and the radial tires.

Machine design factors include flexibility in the structure and the use of a flat belt interposed between the two tires. The vertical load was the same in all tests, and corresponding structural deflection would have the same effect irrespective of the tire being tested. The traction forces were less than 150 N and corresponding deflection would not be significant.

The reason for considering the use of a flat belt as the possible cause of the discrepancies is that if the vertical pressure distribution in the contact patches is different for the two tires, then the belt will deform as it passes through the contact area. This was originally considered only as it affected the energy loss in the tire. It was concluded that, in the worst case, the increase in energy loss compared with that of a flat surface would be no worse than if the tire were running on a 1.7-m-diameter drum. However, the deformation may also change the inclination of the net compressive force vector acting on the tire. An asymmetric longitudinal shift of the center of pressure in the two contact patches will cause such a change in vector inclination, and the longitudinal (traction) force transducer will measure the sine component of the vector.

Appendix B presents an analysis which demonstrates that the pressure distribution in the contact patch of a tire is a function of the internal energy loss and the elastic characteristics of the tire. The analysis assumes

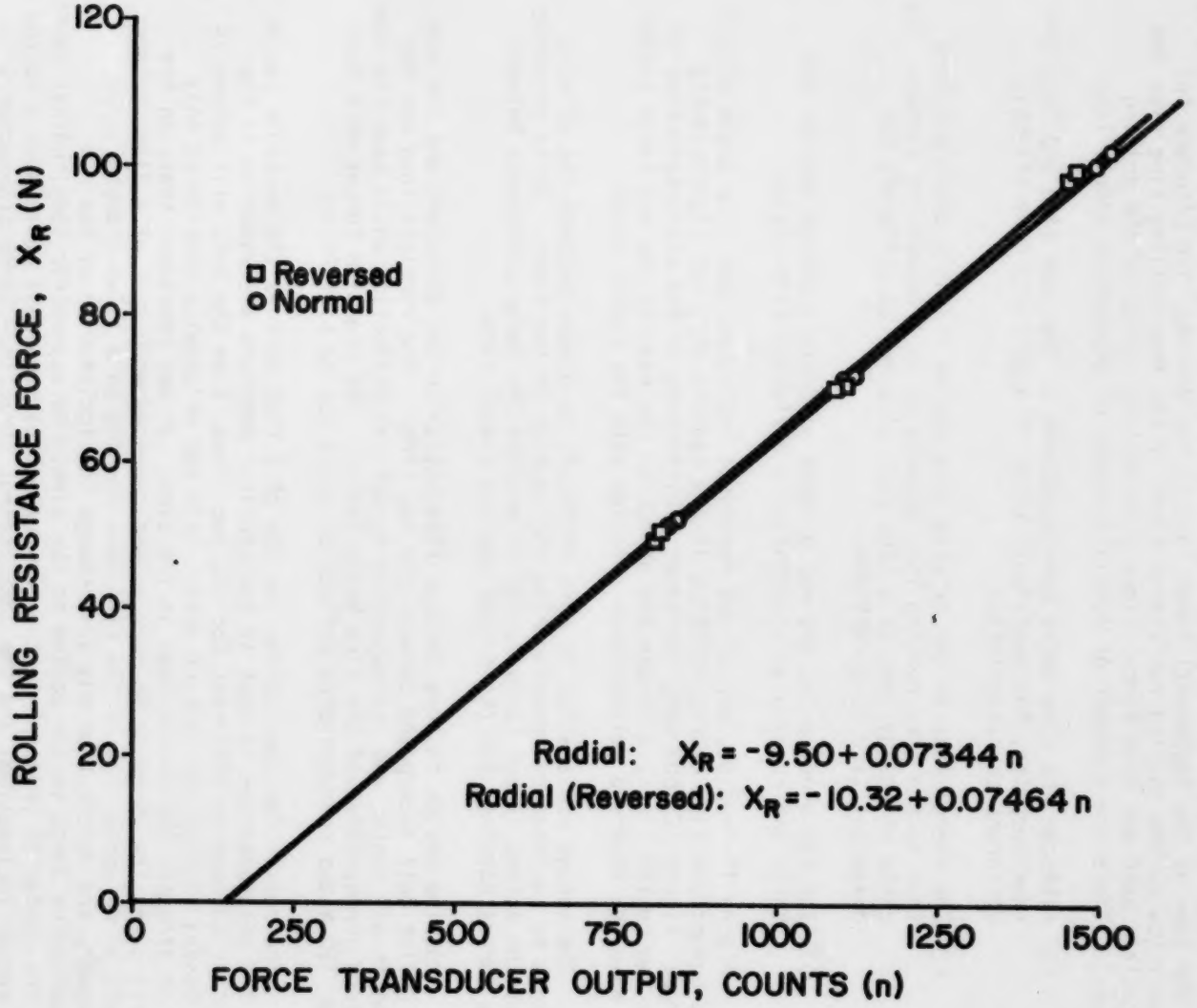

Figure 11. Results of Force Transducer Calibration, Additional Radial Tire Tests in Set 3. Ambient Temperature = 25.6°C.

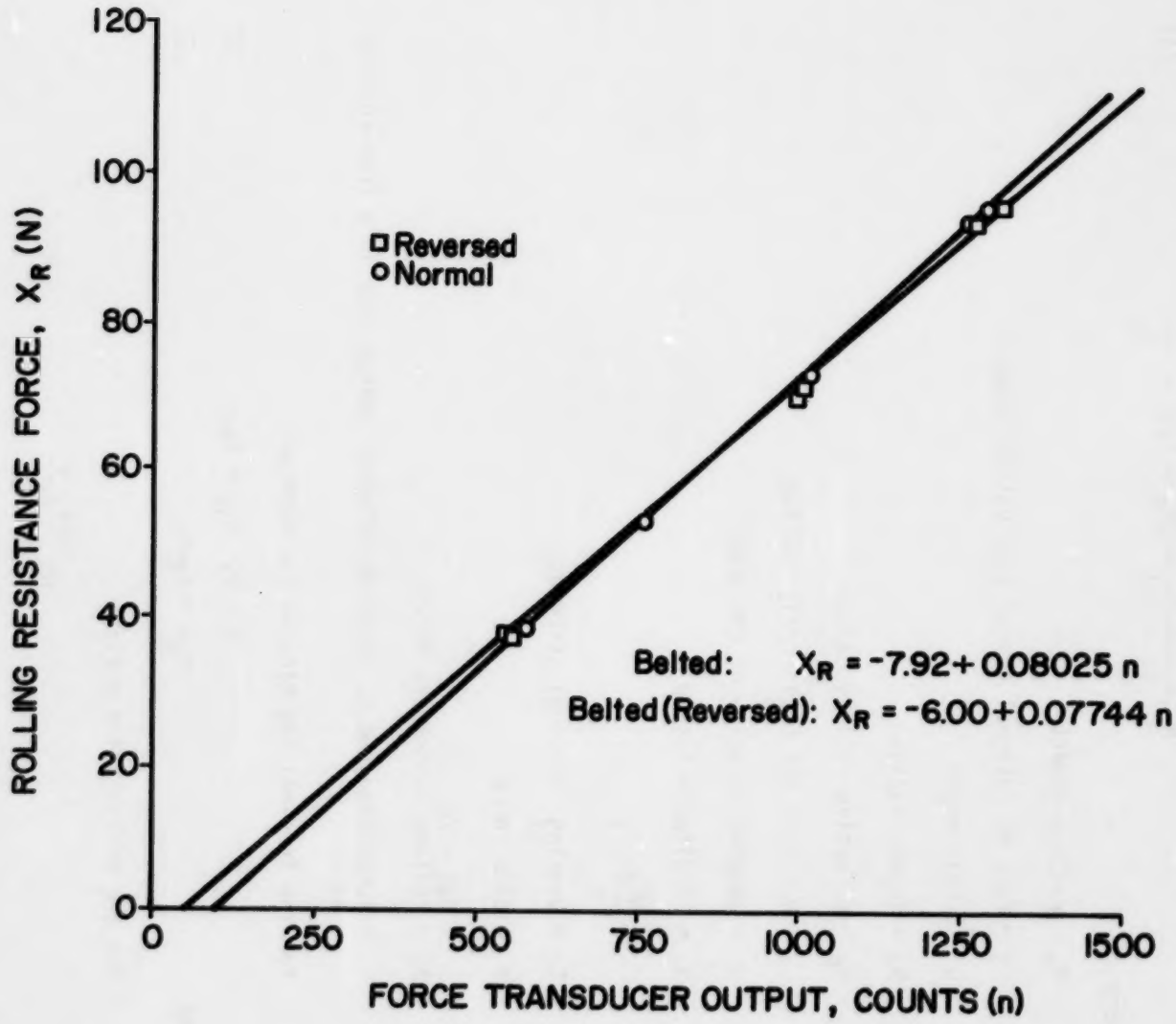

Figure 12. Results of Force Transducer Calibration, Additional Belted Tire Tests in Set 3. Ambient Temperature = 25.6°C.

that the tire is rolling on a flat, rigid surface, which is not true of the flat-belt test machine. The use of Z·e for rolling moment is therefore replaced here by the term M_y.

Equations 6 and 8 in Appendix B give, for operation in the linear range, the expression:

$$M_y = \frac{R_e P_I}{(S + 1)U} + (R_e - R_\ell)X - \frac{R_e X^2}{C_s} \qquad (1)$$

where:

M_y = rolling moment

P_I = rate of internal energy dissipation (power)

U = belt speed

R_ℓ = loaded radius

R_e = effective rolling radius

= U/ω with the tire freely rolling

ω = angular velocity of the wheel

S = longitudinal slip

= $\frac{\omega R_e}{U} - 1$

C_s = braking (driving) stiffness

X = tire force

= $C_s S - X_R$

X_R = rolling resistance force

= force required to overcome internal energy loss in a free-rolling tire

For the free-rolling tire on the machine:

$$S = 0, \quad P_{IF} = X_{RF} U \qquad (2)$$

and

$$M_{yF} = X_{RF} R_\ell \qquad (3)$$

For the driving tire define:

$$T_{RD} = X_{RD} R_\ell$$

where

T_{RD} = rolling resistance torque

= torque required to turn the tire when driving (braking) force is equal to zero

X_{RD} = effective (apparent) rolling resistance force in the ground plane

The power required to overcome rolling resistance torque is therefore:

$$T_{RD}\omega = X_{RD}R_{\ell}\omega = X_{RD}\frac{R_{\ell}(S+1)U}{R_e}$$

Assuming that the energy dissipated in the driving tire due to the extra force transmitted to drive the roadway and the freely rolling tire is negligible compared with the rolling resistance energy loss, the internal power loss is:

$$P_{ID} = X_{RS}\frac{R_{\ell}(S+1)U}{R_e} \tag{4}$$

also,

$$X = X_{RF} + X_B \tag{5}$$

where

X_B = force required to drive the roadway

Now substituting equations 2 and 3 into equation 1 gives

$$M_{yD} = X_{RD}R_{\ell} + (R_e + R_{\ell})(X_{RF} + X_B) - R_e\frac{(X_{RF} + X_B)^2}{C_s} \tag{6}$$

Typical parameter and variable values are:

X_R = 45 N

R_e = 30 cm

$R_e - R_{\ell}$ = 1.0 cm

X_B = 15 N

C_s = 125 kN/unit slip

Note that if $P_{IF} = P_{ID}$, then $X_{RF} \neq X_{RD}$. But slip is very small under the conditions that existed in the calibration tests. For example, if

$$X_{RF} + X_{RD} + X_B = 105 \text{ N}$$

then $$S = 105/(125 \times 10^3) = 0.84 \times 10^{-3}$$

and, from equations 2 and 3,

$$X_{RD} = \frac{R_e}{R_\ell} X_{RF}$$

Subtracting equation 2 from equation 6 and substituting for X_{RD} gives

$$M_{yD} - M_{yF} = (R_e - R_\ell) X_{RF} + (R_e - R_\ell)(X_{RF} + X_B) - R_e \frac{(X_{RF} + X_B)^2}{C_s}$$

$$= (R_e - R_\ell)(2X_{RF} + X_B) - R_e \frac{(X_{RF} + X_B)^2}{C_s}$$

Now, substituting the typical values gives

$$M_{yD} - M_{yF} = 1 \times 105 - \frac{30 \times 3{,}600}{125{,}000}$$

$$= 105 - 0.864$$

showing that

$$M_{yD} - M_{yF} \approx (R_e - R_\ell)(2X_{RF} + X_B) \qquad (7)$$

which gives the net moment acting on the belt in the area of the contact patches of the tires. The moment can be represented by a shift of the center of pressure of the driving tire relative to the center of pressure of the freely rolling tire. It can further be postulated that the belt deformation causes a tilt in the lines of action of the net vertical force vectors, as illustrated in Figure 13. The sine component of the driving tire force vector is now measured by the drive force transducer, causing the transducer output to be larger than the value corresponding to the measured input torque.

To check the above analysis, the effective radius and the rolling radius were measured for each of the three tires at an internal pressure of 165 kPa (24 psi). The resulting values of $(R_e - R_\ell)$ were as follows:

Tire	$(R_e - R_\ell)$, cm
Bias-belted	0.37
Bias	0.55
Radial	1.53

Equations 1 and 7 indicate that, for small drive forces, the error is a linear function of $(R_e - R_\ell)$. A compensation equation may therefore be suggested:

$$X_c = X_{cm} - K(R_e - R_\ell)$$

where

X_c = "correct", or "true", force transducer output (in V/F counts) corresponding to the value of X_R calculated from the torque transducer output

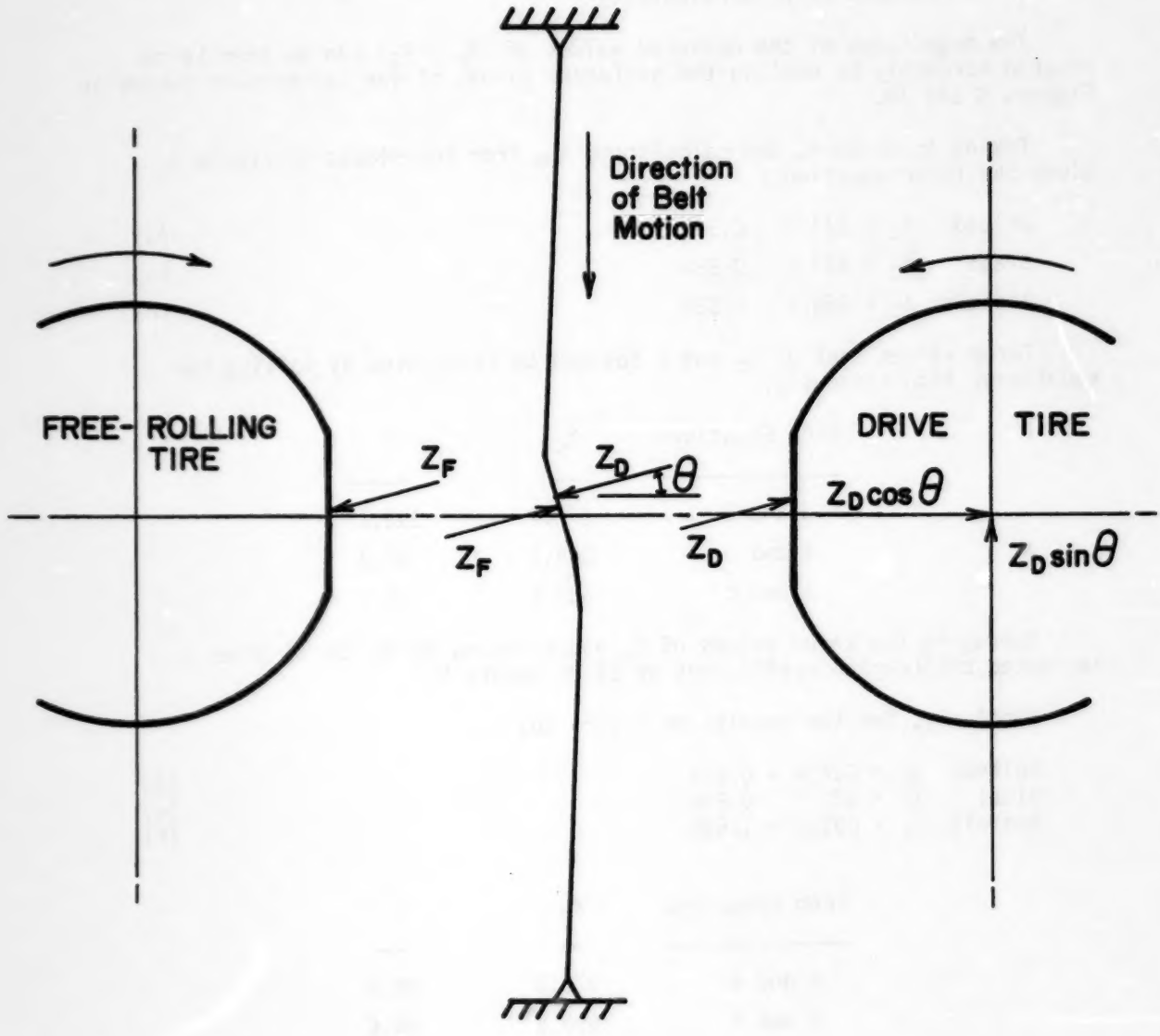

Figure 13. Simplified Schematic of the Belt/Tire System. Deformation of the belt is shown greatly exaggerated. The corresponding deformation of the tire contact patches is not shown.

X_{cm} = measured force transducer output

K = constant of proportionality

The magnitudes of the measured values of $(R_e - R_\ell)$ can be seen to be ordered correctly to explain the different slopes of the calibration curves in Figures 8 and 10.

Taking X_R as 50 N, and calculating X_{cm} from the slopes of Figure 8, gives the three equations:

Belted: $X_c = 611.7 - 0.37K$ (a)

Bias: $X_c = 631.9 - 0.55K$ (b)

Radial: $X_c = 666.4 - 1.53K$ (c)

Three values each of X_c and K now can be calculated by solving two equations, simultaneously.

From Equations	X_c	K
a and b	570.2	112.2
a and c	594.3	47.2
b and c	612.5	35.2

Averaging the three values of X_c and dividing by X_R (50 N) gives a corrected calibration coefficient of 11.85 counts/N.

Similarly, for the results of Figure 10:

Belted: $X_c = 614.9 - 0.37K$ (d)
Bias: $X_c = 632.7 - 0.55K$ (e)
Radial: $X_c = 692.2 - 1.53K$ (f)

From Equations	X_c	K
d and e	578.3	98.9
d and f	590.3	66.6
e and f	599.3	60.7

and the corrected calibration coefficient is 11.79 counts/N.

When calibrating the force transducer with dead weights, calibration coefficients in the range 11.6 to 12.5 counts/N were obtained. The corrected coefficients tend to compare more favorably with the dead weight results than do the coefficients in Figures 8 and 10. As an indication of the small deflections involved, the correction to the force measurement in equation (f) was approximately 100 counts, equivalent to 8.5 N. For a vertical load of 3.7 kN, this represents a rotation of the load vector of just 8 minutes of arc.

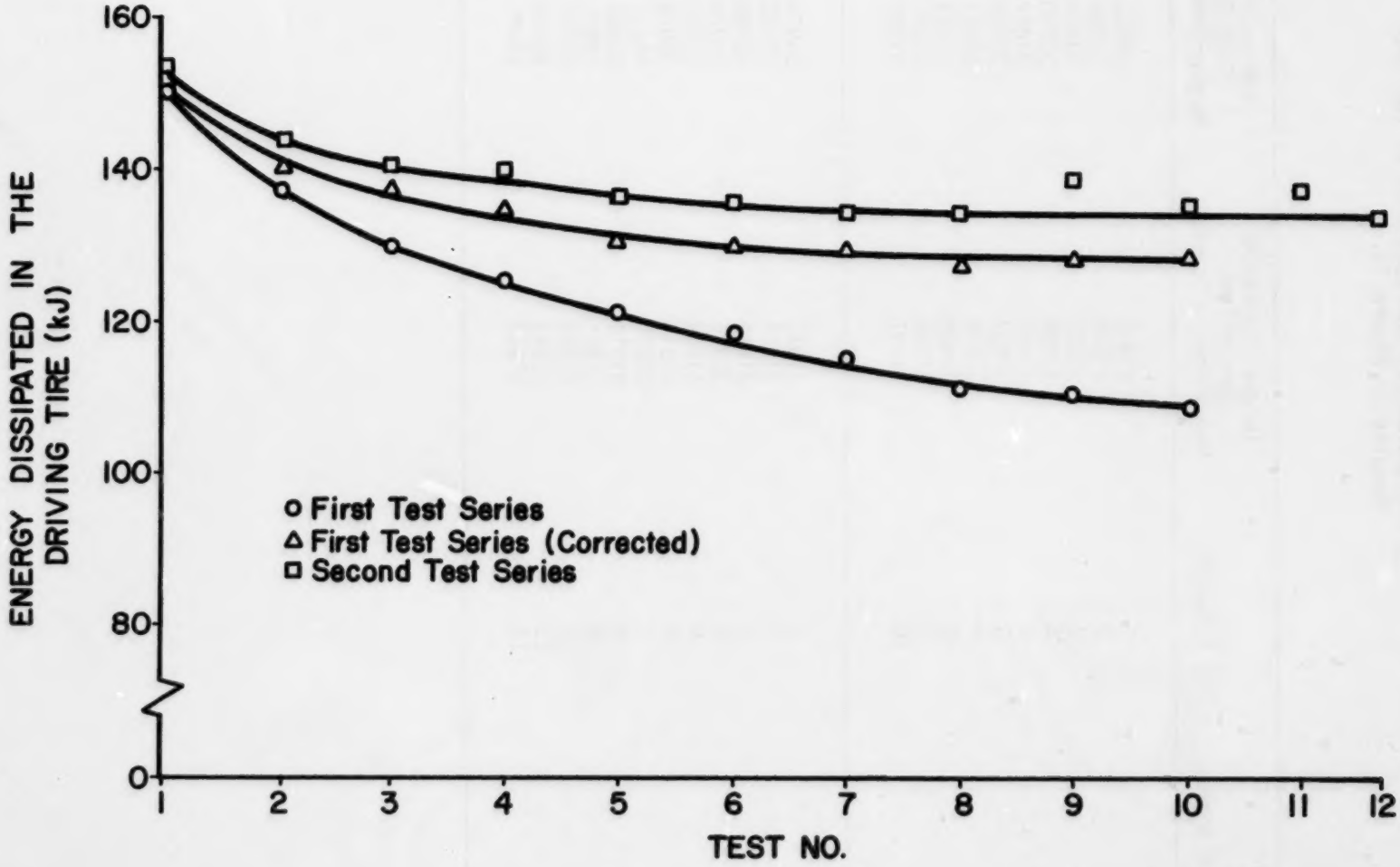

Figure 14. Energy Dissipated in the Driving Tire Over the Transient Segment of the EPA Urban Cycle (vertical scale expanded)

Table 3. Force and Torque Transducer Zero Offset Measurements Corresponding to the Test Results in Figure 14.

Test Series	Test Number	Torque Transducer Zero Offset Measurement, Counts	Force Transducer Zero Offset Measurement, Counts
1	1	31910	30988
	2	31910	31006
	3	31909	31031
	4	31909	31040
	5	31908	31042
	6	31907	31056
	7	31908	31071
	8	31909	31079
	9	31909	31091
	10	31907	31102
2	1	31913	30979
	2	31914	30980
	3	31914	30986
	4	31916	30979
	5	31918	30980
	6	31914	30978
	7	31915	30982
	8	31911	30982
	9	31911	30978
	10	31912	30982
	11	31913	30988
	12	31913	31001

The above analysis has attempted to show that the force transducers on the machine are subject to an error which is a function of the tire (and belt) properties. To accurately describe the deformation characteristics of the tires and belt in the contact area would be an extremely difficult problem, and general arguments were used to predict the nature of the belt deformation. Whether or not the arguments are correct, the numerical results tend to indicate the presence of an error which is a linear (or nearly so) function of the tire parameter $(R_e - R_\ell)$.

3.7 Energy Measurements

Despite the problems encountered with temperature drift and the calibration of the force transducers, a number of tests were run to obtain an estimate of the performance of the machine when measuring tire energy dissipation. To reduce the effects of temperature drift, the individual test runs were of relatively short duration and consisted of operating the machine over the transient segment of the EPA urban cycle, with a maximum speed of 37.5 km/h. C-14 tires were used with a total inertial load of 320 kg.

In the first series of tests, a radial tire was run over ten successive cycles and the energy dissipated in the driving tire was computed for each cycle. The procedure was to run the machine at low speed with the tires unloaded and to measure the zero offset values of the transducer outputs, averaged over 60 seconds. The tires were then loaded and the transient cycle executed. At the conclusion of the cycle the tires were unloaded, the zero offset values were measured, and another cycle was run. Figure 13 shows a plot of the measured energy dissipation over succeeding cycles, and Table 3 lists the force and torque transducer zero offset values. The torque transducer offset was extremely stable, but the force offset drifted by approximately 9 N from the first to the last test. This represents a voltage offset on the input to the force/belt multiplier, causing an error in the measurement of the energy flowing out of the tire. An estimate of the error was made by computing the effective energy dissipation of the offset force acting over the cycle. The error was then added to the measured energy dissipation in the tire, giving the corrected curve shown in Figure 14.

The same test procedure was repeated at a later date, but the force transducer offset voltage was adjusted to zero at the beginning of each test. The results from this and the previous series of tests compare well (see Figure 14 and Table 3). There is a difference in the measured energy dissipation of 1.6 percent in the first test and 3.8 percent in the last test. The fluctuation in the last few tests of the second series was caused by an interruption in the test procedure and some changes in the time elapsing between individual tests. Apart from machine errors, differences in the measured results would be due to differences in the ambient condition and tire pressures, and to errors in the correction made to the results of the first series.

A further series of tests was run with all three tires (belted, bias, and radial), in which the energy dissipation over the transient cycles was measured for each tire on two different days. The tires were soaked for 24 hours prior to each test. Table 4 summarizes the results obtained. The "static" calibration results were computed using a dead weight calibration

Table 4. Energy Flow During The Transient Segment of the EPA Urban Cycle (Maximum speed = 37.5 km/h, inertial load = 320 kg)

TIRE	TOTAL ENERGY ENTERING THE DRIVING TIRE ω.T, (kJ)	ENERGY LEAVING THE DRIVING TIRE U.X (kJ)			ENERGY DISSIPATED IN THE DRIVING TIRE ω.T-U.X (kJ)		
		Static Calibration	Dynamic Calibration		Static Calibration	Dynamic Calibration	
			Fig. 8	Fig. 10		Fig. 8	Fig. 10
Radial	553.5	322.5	307.3	291.1	231.0	246.2	262.5
	550.0	315.8	301.0	285.1	234.1	249.0	264.9
Bias	540.0	295.2	291.6	291.6	244.8	248.4	248.4
	548.9	298.3	294.6	294.6	250.6	254.3	254.3
Belted	586.6	300.6	306.7	305.4	286.0	279.9	281.2
	590.1	308.4	314.7	313.3	281.7	275.4	276.8

Note: The dynamic calibration results were found by using the calibration coefficients from Figures 8 and 10.

coeffieicent and the "dynamic" calibration results were computed using the the calibration coefficients of Figure 8 and 10. A series of rolling resistance force measurement tests were also run in conjunction with the energy dissipation tests. A light load test was run first, and the force at the belt surface calculated from the torque transducer output and the rolling radius (R_ℓ). Then a rated load test was run at constant speed for a period of 30 minutes with the torque transducer output measured at intervals of approximately 5 minutes and divided by the rolling radius. Rolling resistance force was then calculated by subtracting the light load force from the rated load force measurements. Figure 15 shows the results.

Table 5 summarizes the rolling resistance force and energy dissipation test results by referencing the belted and bias-ply tire performance measures to the radial-ply tire performance. (Relative performance is the belted/bias performance measure divided by the radial performance measure.) Except for showing a reasonable correspondence between the energy dissipation measurements and the rolling resistance force measurements, the results are somewhat ambiguous and definite conclusions cannot be drawn from them. However, the importance of having accurate calibration coefficients is apparent.

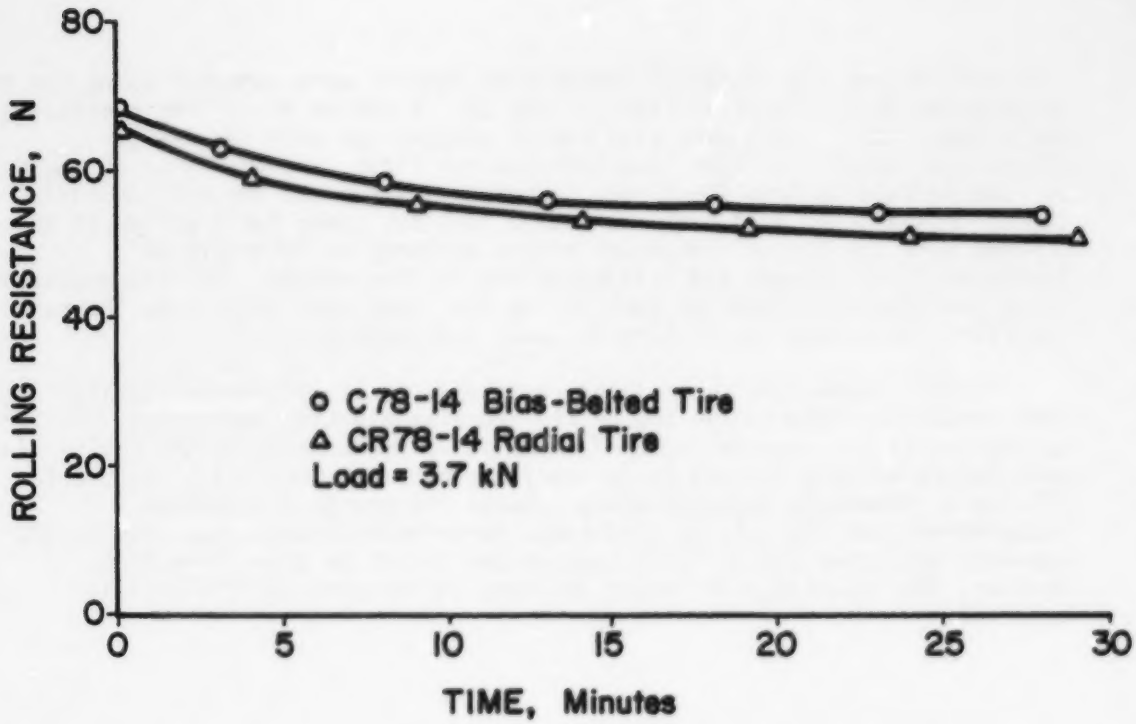

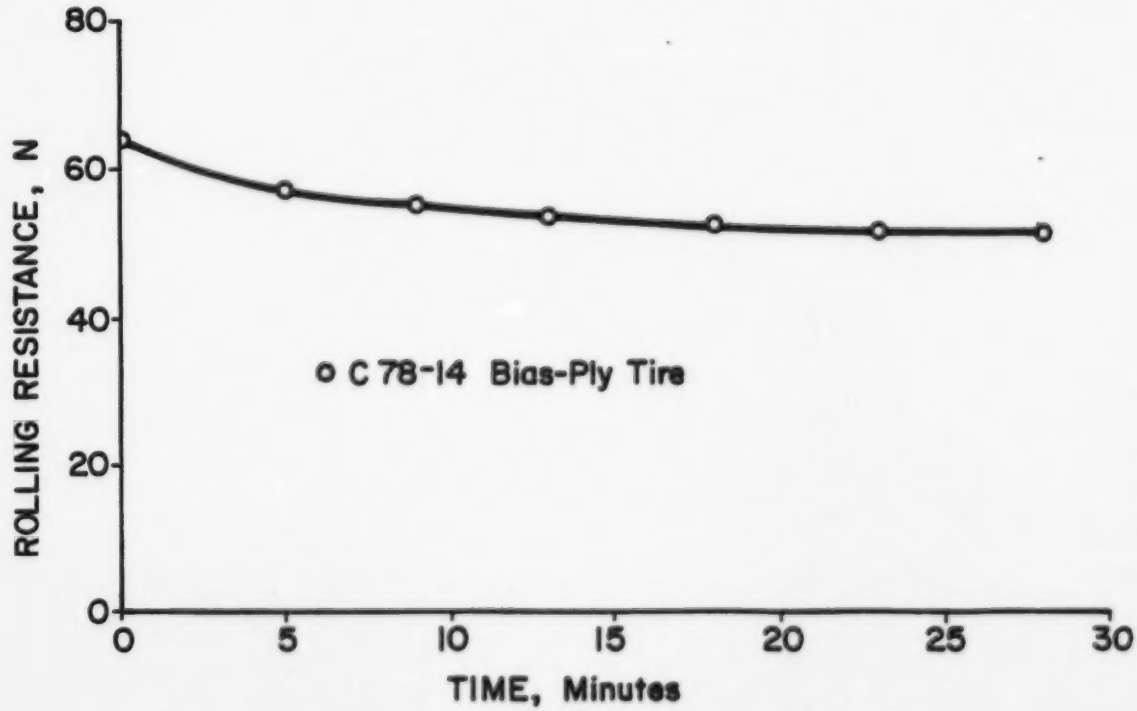

Figure 15. Constant Speed Rolling Resistance Test Results

Table 5. Performance of Bias and Belted Tires Relative to the Radial Tire for Different Test Measurements

Test Measurement	Performance Relative To The Radial Tire	
	Bias	Belted
Energy Dissipated In the Driving Tire		
Static Calibration	1.07	1.22
Dynamic Calibration (Fig. 8)	1.01	1.12
Dynamic Calibration (Fig. 10)	0.95	1.06
Total Energy Entering the Driving Tire	0.99	1.07
Rolling Resistance at T = 0	0.96	1.02
Rolling Resistance at T = 25	1.01	1.07
Average Over the Constant-Speed Rolling-Resistance Tests	1.00	1.06

4. SUGGESTED MODIFICATIONS

A number of modifications could be made to either the machine or the test procedure to improve the accuracy of energy dissipation measurement. These are discussed below in increasing order of likely improvement in accuracy.

4.1 Individual Force Calibration

Using the dynamic calibration procedure described previously, determine force transducer calibration coefficients for each tire tested. This would be time consuming and introduce a new calibration precision error for each tire tested. Also, since the operating conditions (mainly tire pressure) during calibration are not the same as during a test, an error of unknown magnitude would be introduced.

4.2 Corrected Force Calibration

Determine the "true" force transducer calibration coefficients by (a) running dynamic calibrations for a number of tires, (b) measuring $(R_e - R_\ell)$ for each tire at each tire pressure used in the calibrations, and (c) calculating the average of the values X_c in the equations corresponding to equations (a) through (f) given previously. Now, each time a new tire is tested, $(R_e - R_\ell)$ would be measured at the test inflation pressure and the force transducer measurement corrected in the data reduction program with the equation:

$$X = k_c(X_{cm} - K(R_e - R_\ell))$$

where

X = corrected force measurement (N)

X_{cm} = measured force transducer output (counts)

K = average of K values in the equations corresponding to equations (a) through (f)

k_c = calibration coefficient computed from the X_c values obtained at each tire pressure

This procedure would be prone to errors of the kind introduced by the first modification. Note also that $(R_e - R_\ell)$ will vary with inflation pressure and will thus vary during a test.

4.3 Indirect Measurement of Roadway Losses

Measure the total energy entering the system from the drive shaft torque transducer and the motor speed transducer outputs. Subtract from this measurement an estimate of the roadway energy dissipation calculated from measurements of effective roadway resistance force made before and after the main energy dissipation test. The roadway resistance force could be measured in run-down tests from the maximum speed, with the tires unloaded, and using the expression.

$$X_{BR} = \frac{1}{m} \cdot \frac{du}{dt} = \frac{1}{m} \frac{(U_1 - U_2)}{(t_2 - t_1)}$$

where

X_{BR} = effective roadway resistance force

m = effective inertia

U = belt speed

$(U_1 - U_2)$ = change in belt speed over time $(t_2 - t_1)$

The energy dissipated by the roadway over one cycle is then computed from the estimated values of X_{BR}, and the belt speed is measured during each one-second portion of the cycle.

Excluding the losses in the flywheel gearbox, the major component in the roadway losses is probably that due to bearing friction. For example, assuming a bearing coefficient of friction of 0.001 to 0.002, the effective bearing resistance force at the belt surface can be calculated as being in the range 15 to 30 N. From a run-down test in which the time between two speeds was measured with a stop watch, and also from the calibration tests, the roadway resistance force at the belt was found to be approximately 15 N. The good correspondence between the calculated and measured values indicates that the bearing losses are dominant and thus that the roadway losses are not strongly dependent on belt speed. Measuring belt speed over fairly long intervals of time should therefore give a good estimate of the effective resistance force, although error bounds and expected variation during a test cannot be given without further tests being made on the machine. Adding the flywheel and gearbox, however, would increase the speed dependence, because of oil churning and hydrodynamic friction, and would introduce load dependence because of torque transmission losses.

4.4 Equal Torque Drive

In this, the most drastic of the modifications, the machine is reworked so that equal and opposite torques are applied to both wheel axles. Thus, the two tires would experience the same pressure distribution in their contact patches, apart from differences caused by manufacturing tolerances, and the belt would suffer no deformation. The most straightforward redesign would be to add a complete drive shaft, torque transducer, and drive motor assembly to the (presently) free-rolling-wheel assembly. Torque control of the motors would be necessary. A less expensive method would be to add the extra drive shaft and torque transducer and split the drive from the motor to the wheel axles through a differential. In this configuration speed control would still be possible. The only functional difference in the machine, compared with the present configuration, would be that a complete half car would not be simulated.

A more flexible arrangement could be obtained if the speed-controlled motor were used to drive the lower drum and a torque-controlled motor used to drive the wheels. Full simulation of vehicle characteristics would then be possible since aerodynamic and inertia forces could be generated by the wheel drive motor and speed controlled by the drum motor. Additionally, constant drive torque and constant belt speed tests could be run, which would allow the effect of drive torque on tire energy dissipation to be determined directly. It might then be possible to estimate tire energy dissipation over a given driving cycle from a suitable mapping of results from the constant-torque, constant-speed tests.

4.5 Free-Rolling Resistance Force Measurements

In its present configuration, the machine is capable of providing precise measurements of free-rolling resistance force if the torque transducer output is used and a skim test run to determine the parasitic losses. The skim test probably introduces the most error into the test technique, but there is also some uncertainty about the validity of assuming that the energy losses in the driving and freely rolling tires are equal. The fact that the driving tire also supplies the energy for roadway motion introduces an error that is probably slight. Bearing friction losses are difficult to determine since the skim test measures only the light load friction.

Elimination of the skim test and the equal energy loss assumption would, however, be possible by the relatively simple modification of driving the lower drum instead of one of the wheels. Roadway losses could then be measured simply by running the machine with the tires unloaded. Bearing losses would then be the only significant source of error.

5. CONCLUSIONS

A machine has been developed to simulate a vehicle traveling over transient driving cycles representative of typical consumer passenger vehicle usage for the purpose of obtaining information on the energy dissipated by the tires of a vehicle over such cycles. The main feature of the machine is that two tires are loaded against each other across a steel belt. One of the wheels is driven to follow the required driving cycle, and the other wheel is allowed to roll freely. The energy dissipated in the driving tire is measured by subtracting the energy leaving the tire from the energy entering the tire. The machine meets the first project objective in all but two aspects. The first is that temperature drift in the force transducer outputs is unacceptably large. This can be corrected. The second is that an unacceptably large error exists in the tire force measurements which is independent of the transducers and the signal conditioning circuits. The error probably arises from small deformations in the belt and is a function of the construction of the tires installed on the machine. It cannot be eliminated, or corrected for, with the machine in its present configuration.

A number of modifications to the machine and the test procedures have been suggested to improve the accuracy of the energy dissipation measurements. Further developmental work is required to test the validity of the modifications. In its present configuration, however, the machine can be used to accurately measure the energy dissipated in tires under free-rolling conditions.

REFERENCES

1. Cassidy, R. J., ed. "A Feasibility and Preliminary Design Study of an Advanced Tire Force and Moment Test Facility." Report No. YD-2639-K-1R. Cornell Aeronautical Laboratory, Nov. 1969.

2. Schuring, D. J. "Energy Loss of Pneumatic Tires Under Freely Rolling, Braking, and Driving Conditions." Tire Science and Technology, Vol. 4 (1976), pp. 3-15.

3. Gough, V. E., "Tyre-to Ground Contact Stresses." Wear, Vol. 2 (1958-1959), pp. 107-126.

4. "Vehicle Dynamics Terminology, Recommended Practice J607d." Society of Automotive Engineers, 1975.

5. Dugoff, H., Fancher, P.S., and Segel, L. "An Analysis of Tire Traction Properties and Their Influence on Vehicle Dynamic Performance." SAE Paper 700377. Society of Automotive Engineers, 1970.

6. Schuring, D. J., Bird, K. D., and Martin, J. F., "Power Requirements of Tires and Fuel Economy." Tire Science and Technology, Vol. 2 (1974), pp. 261-285.

7. Hussman, A. W. and Gerresheim, M. "Normal and Shear Forces and Actual Slippage in the Contact Area of Tires." Paper presented to Japan Society of Automotive Engineers, October 1973.

APPENDIX A
MACHINE COMPONENTS

A.1 Roadway Drums

The drums were manufactured from Dodge 30 x 18 in. (762 x 457 mm) straight K50 taper-lock steel conveyor pulleys, standard except for 5/8-in. (15.88-mm) rim thickness. The shaft is 4-15/16 in. (30.34 mm) diameter, keyed and taper-locked to the shaft. The drums were machined to the dimensions shown in Figure A-1, and then dynamically balanced.

A.2 Roadway Belt

The belt is a Sandvik stainless steel conveyor belt, 16 in. (406.4 mm) (15.75 in. [400 mm] actual) wide by 0.032 in. (0.81 mm) thick, welded to an endless length of 218 in. (5.54 m).

Apart from the accidental breaking of one belt, belt performance was found to be satisfactory. Tire to belt friction was high and showed no apparent degradation with use. Although the tires were run-in on the road for 320 km, some flash remained in the tread area which tended to wear off and attach itself to the belt and drums. The main effect was to cause the belt to adhere to the drum and to excite small amplitude vibrations in the free-span of the belt. The rubber deposits were cleaned off periodically and were not considered a serious problem.

Small amplitude free-span vibrations were also excited in the belt by the welded joint, which had not been uniformly dressed flush with the belt surface. Where it protruded above the belt surface, the weld material underwent plastic working, but the nonuniformity was not completely eliminated. Careful dressing of the weld on the inside of the belt should have been specified when the belt was ordered.

A.3 Inertial Load Drive

A Dodge torque-arm single-reduction speed reducer (size T-14), with 5.27 gear ratio, is used in the inertial load drive. The lower drum shaft was machined to the speed reducer output bore size and the speed reducer mounted directly on the shaft. The inertial load flywheels are directly mounted on the speed reducer output shaft. A sectioned view of the speed reducer is shown in Figure A-2.

A.4 Effective Inertia of the System

The effective inertias (mass at the belt surface) of the drums and belt are 309 kg and 14.3 kg respectively. The total effective mass of the machine with the inertial load drive demounted is therefore 313.3 kg. Additional inertial loads can be calculated from Table A-1.

A.5 Flexible Coupling

The coupling located between the force transducer and the motor drive shaft is a Thomas Series 52 metallic high-speed coupling, size no. 262. Dimensions and data are given in Figures A-3 and A-4.

Table A-1. Tire and rim association passenger tire load ratings with corresponding inertia loads required to simulate one half of a car on the machine.
(Required inertial load = twice 80% rated load divided by gravity constant)

Rated Tire Load Designation	Rated Tire Load lb (kg)	80% Rated Tire Load lb (kg)	Required Inertial Load kg
A	900 (408)	720 (327)	654
B	980 (445)	784 (356)	712
C	1050 (476)	840 (381)	762
D	1120 (508)	896 (406)	812
E	1190 (540)	952 (432)	864
F	1280 (581)	1024 (464)	928
G	1380 (626)	1104 (501)	1002
H	1510 (685)	1208 (508)	1096
J	1580 (717)	1264 (573)	1146

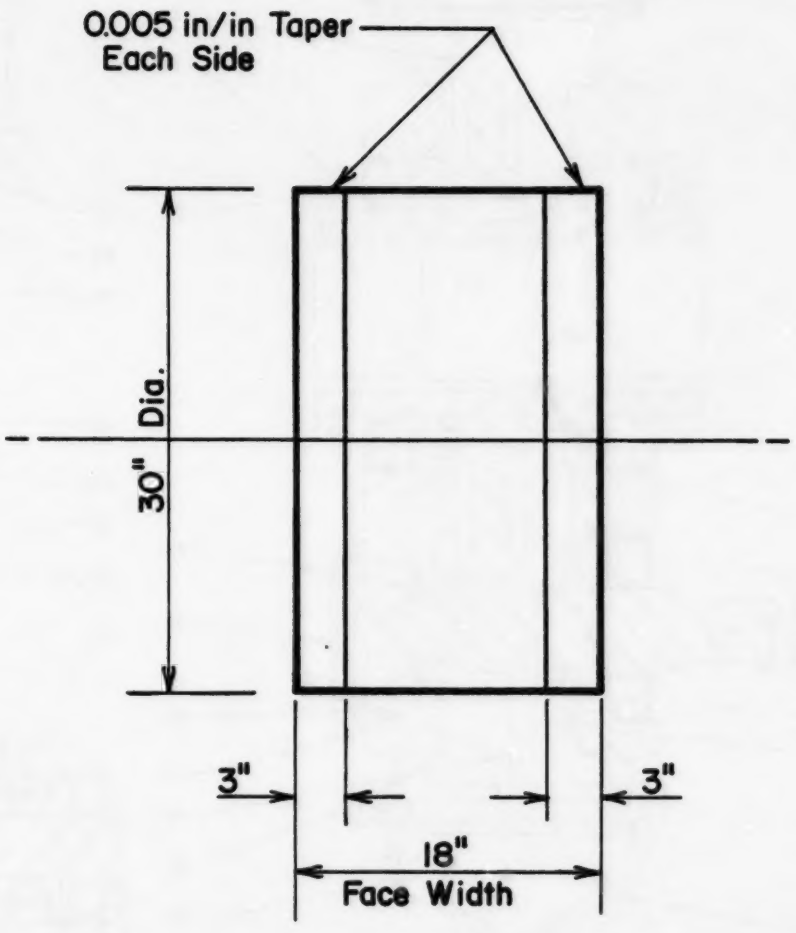

Figure A-1. Roadway Drum Dimensions

PARTS FOR T14 STRAIGHT BORE SPEED REDUCERS

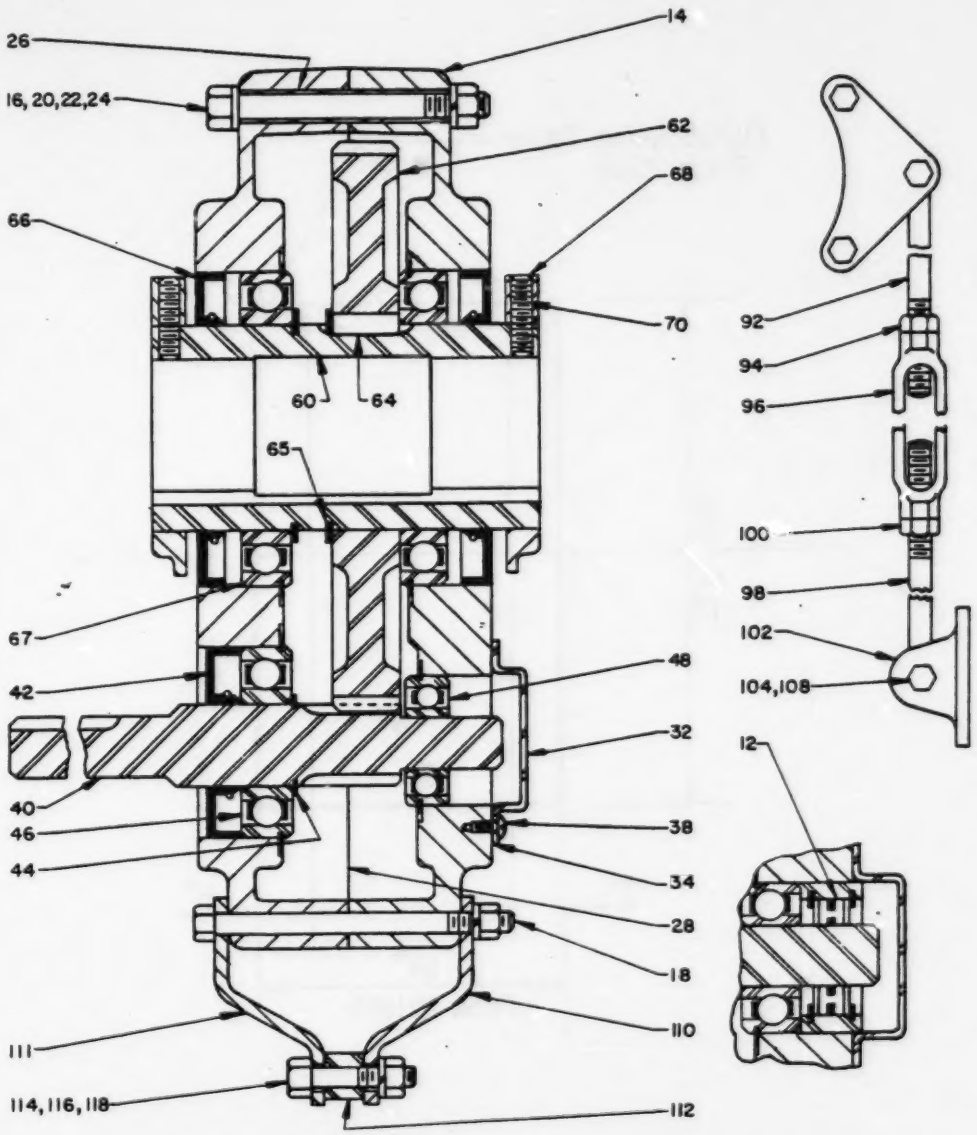

NOTE: The two digit numbers are for reference only. Order parts by the six digit numbers in the Price List. Each six digit number is a complete identification of the part or assembly.

Figure A-2. Inertial Load Drive Speed Reducer

THOMAS HIGH SPEED COUPLINGS

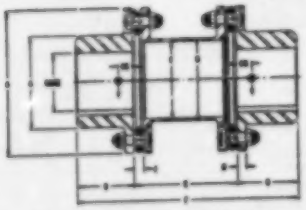

Dimension G varies with bore specified

SERIES 52

Series 52 couplings have been adopted as the standard for high-speed process and refinery pumps by many major manufacturers in the hydrocarbon processing industry. They have also seen wide usage on large boiler pump drives in the power generating industry.

The Series 52 coupling should be considered as an economical selection for drive systems where the extremely light weight of the Series 63 coupling is not necessary and where operating speeds are within the published limits of the Series 52 design. Hubs and center member are manufactured from carbon steel with careful control being exercised over the heat treatment of the raw material. Bolts are made of high-strength alloy steel to provide adequate clamping action, with the bolt body ground to precision tolerance so that dynamic balance is achieved and maintained throughout the life of the coupling. The flexing elements may be furnished in either Tomalov (modified carbon steel) or 300-series stainless. The latter material is recommended for corrosive environments, outdoor operation, and where an extra margin of reliability is desired.

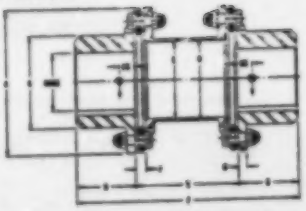

Dimension G varies with bore specified

SERIES 53

The details of construction for the Series 53 coupling are similar to the Series 52 except that the flanges are "slabbed" to reduce coupling weight by 12-18%. This coupling is an ideal selection for applications requiring a slight weight reduction from the Series 52 values but where economics do not permit use of the Series 63. It is also suitable for drives which require minimum coupling weight but where the size of connected shafts (rather than load capacity) dictate the coupling size selection. The Series 53 has been widely applied to process and boiler feed pumps and to high-speed compressor drives.

A significant characteristic of Series 52 and 53 couplings is that the stiffness of these types, under conditions of misalignment and axial motion, is substantially lower than the Series 63 design. The stiffness is also lower than virtually any other type of flexible coupling available which can have an appreciable effect on service life of bearings and seals on connected equipment.

Series 53 couplings (and Series 52), because of their inherent design features, have a characteristically high torsional stiffness which is desirable for many drive systems. However, substantial reductions (of up to 400%) in torsional stiffness can be achieved, without increased shaft separation, by modifications to the coupling center member. Consult Rexnord for design proposals to suit these requirements.

TABLE 7

MAXIMUM HP PER 100 RPM

Size No.	Service Columns 2	3	4
162	3.0	3.0	1.7
200	5.9	3.8	3.3
225	8.6	5.7	4.8
262	14.9	9.9	8.3
312	26.0	16.6	13.3
350	33.5	22.4	18.6
375	39.7	26.5	22.7
425	52.0	45.3	37.7
450	57.5	38.4	46.7
500	150	88.3	74.4
550	196	131	109
600	274	182	152
700	427	285	235
750	548	383	318
800	697	464	387
850	865	577	481
925	1160	775	644

GENERAL DIMENSIONS (Inches)

Size No.	Max. Bore	Max.[3] R.P.M.	A	B	Std. C[3]	D	E	F	G[1]	H	J	CG
162	1.75	30,000	4.34	1.75	5.00	2.44	2.25	8.50	2.75	23	26	Consult Rexnord
200	2.56	24,600	5.44	2.06	5.00	3.12	2.94	9.13	3.26	28	36	
225	2.44	23,300	5.69	2.44	5.00	3.25	3.06	9.88	3.78	28	36	
262	2.88	20,400	6.62	2.88	5.00	3.75	3.50	10.75	4.50	36	47	
312	3.38	17,300	7.81	3.38	5.50	4.50	4.25	12.25	5.25	41	50	
350	3.75	15,500	8.69	3.75	6.00	5.00	4.75	13.50	5.88	47	53	
375	4.13	13,900	9.69	4.00	7.00	5.50	5.19	15.00	6.50	55	58	
425	4.50	12,800	10.50	4.25	7.00	6.00	5.62	15.50	7.00	61	61	
450	4.75	11,900	11.31	4.50	8.00	6.38	6.00	17.00	7.44	66	71	
500	5.38	10,400	12.88	5.00	9.00	7.25	6.81	19.00	8.38	77	77	
550	6.00	9,200	14.44	5.50	10.00	8.12	7.50	21.00	9.44	88	80	
600	6.50	8,400	15.00	6.00	10.00	9.00	8.38	22.00	10.25	88	97	
700	7.50	7,300	18.25	7.00	11.00	10.00	9.25	25.00	11.75	1.16	1.19	
750	8.00	6,700	19.81	7.50	11.00	11.00	10.12	26.00	12.63	1.25	1.30	
800	8.75	6,200	21.50	8.25	12.50	12.00	11.00	28.50	13.63	1.38	1.37	
850	9.25	5,800	23.00	8.75	13.00	12.75	11.75	30.50	14.50	1.47	1.39	
925	10.13	5,400	25.00	9.50	14.00	13.81	12.69	33.00	15.75	1.63	1.48	

1. "G" dimension at maximum bore.
2. Dynamic balancing is necessary for high speed service. Consult Dynamic Balancing Guide on Page 2.
3. Standard Dimension—may be increased as necessary.

Rexnord

Note: Catalog dimensions may be subject to change or correction. Please request certified prints for current and exact dimensions.

Figure A-3. Flexible Coupling (Series 52)

THOMAS HIGH SPEED COUPLINGS
SERIES 52 AND 53

AXIAL AND ANGULAR STIFFNESS DATA

Estimated Variation In Axial Restoring Force vs Axial Displacement

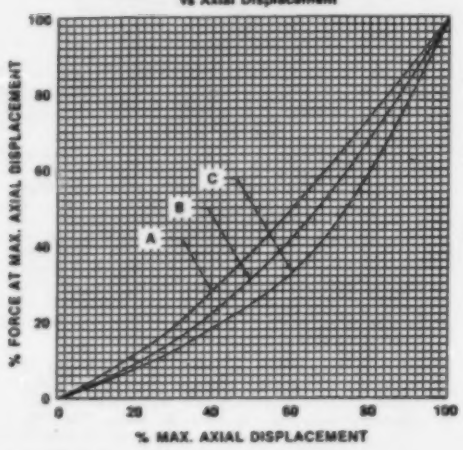

FIGURE 5

To Determine Axial Restoring Force:

1. Determine coupling size and Actual Axial Displacement.
2. Using Step 1 and Maximum Axial Displacement from Table 10, calculate % Maximum Axial Displacement for the given application.
3. With the value from Step 2, determine the % Force at Maximum Axial Displacement from Figure 5 using the designated line for the selected coupling size.
4. The Axial Restoring Force for the application is obtained by multiplying the value obtained in Step 3 by the Maximum Axial Force for the appropriate coupling size as listed in Table 10.

TABLE 10

AXIAL STIFFNESS DATA ①

Size No.	Maximum Axial Displacement (in.)	Maximum Axial Force (lb.)	Line
162	± 0.036	18	A
200	± 0.036	20	A
225	± 0.038	75	A
262	± 0.043	54	A
312	± 0.051	95	A
350	± 0.058	106	B
375	± 0.062	155	C
425	± 0.067	185	C
450	± 0.072	160	B
500	± 0.082	154	B
550	± 0.092	212	B
600	± 0.102	286	B
700	± 0.115	242	C
750	Consult Rexnord		
800			
850			
925			

Special design modifications can be made for conditions requiring greater axial travel and/or lower axial forces. Consult Rexnord with requirements.

1. Values are shown for a complete coupling with two laminated rings. For a single laminated ring, maximum axial travel is one-half the amount shown.

Estimated Angular Restoring Moment vs - Angular Misalignment

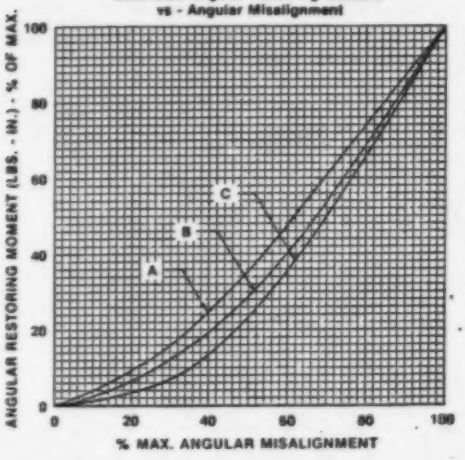

FIGURE 6

To Determine Angular Restoring Moment:

1. Determine coupling size and Actual Angular Misalignment.
2. Using Step 1 and Maximum Angular Misalignment from Table 11, calculate % Maximum Angular Misalignment for the given application.
3. With the value from Step 2, determine the % of maximum Angular Restoring Moment from Figure 6 using the designated line for the selected coupling size.
4. The Actual Angular Restoring Moment is obtained by multiplying the value obtained in Step 3 by the Maximum Angular Restoring Moment for the appropriate coupling size as listed in Table 11.

TABLE 11

ANGULAR STIFFNESS DATA ①

Size No.	Maximum Angular Misalignment Per Flexing Element	Maximum Angular Restoring Moment (lb-in)	Line
162	± 0.33°	5	A
200	± 0.33°	11	A
225	± 0.33°	46	A
262	± 0.33°	36	A
312	± 0.33°	77	A
350	± 0.33°	89	B
375	± 0.33°	74	C
425	± 0.33°	92	C
450	± 0.33°	133	B
500	± 0.33°	142	B
550	± 0.33°	224	B
600	± 0.33°	334	B
700	± 0.33°	187	C
750	Consult Rexnord		
800			
850			
925			

1. Misalignment values shown are for a single flexing element; total shaft-to-shaft misalignment is twice the tabulated value, providing no parallel misalignment is present. Consult Rexnord for misalignment requirements in excess of published maximums.

Note: Catalog dimensions may be subject to change or correction. Please request certified prints for current and exact dimensions.

Rexnord

Figure A-4. Flexible Coupling Stiffness Data

A.6 Motor and Drive

The motor is controlled by a Robicon static reversing, fully regenerative, 6-pulse, 12 SCR DCD motor drive, rated at 50 hp, with 230 V, 3 phase, 60 Hz AC input and 240 V DC output. Speed accuracy of one percent is specified when motor speed feedback is taken from a Powertron XPY tachometer. XPY tachometers are used to measure motor speed and belt speed. Major specifications for the tachometers are: 0.5% RMS ripple, 52 ripple cycles per revolution, and a temperature coefficient of 0.022% FS/°C. The motor is a 50-hp, 1750 RPM, 240 V DC drive motor on a 365 AT frame. The motor drives the wheel driveshaft through a 2:1 toothed-belt speed reduction drive.

A.7 Force and Torque Transducers

The tire force transducers are two-component strain gauge units manufactured by K. J. Law, Inc. (under license from General Motors) for use on ASTM E 217 specification pavement skid testers. Full-scale rated load is 4.5 kN. See Section 2.5 for more information.

The drive shaft torque transducer is a Lebow 1228-10K flange drive unit (Figure A-5). The full-scale rated load is 1.13 kN, the linearity is 0.1% FS, and the zero-offset temperature coefficient is 0.004% FS/°C.

A.8 Signal Conditioning Instrumentation

The instrumentation system was constructed from linear integrated circuits and, where necessary, low-temperature-coefficient passive devices. Critical components, and their functions, are listed below. Specification sheets are given in Figures A-8 through A-14.

AD 581K	Strain gauge bridge excitation voltage reference
AD 521K	Differential input instrumentation amplifier for strain gauge bridge output conditioning
AD 517J	Filter/buffer amplifier
AD 534L	Precision IC multiplier for computing power from force, or torque, and speed voltage signals.
AD 537K	Voltage to frequency converter
AM 7601C	Commutating auto-zero operational amplifier for wheel force transducer preamplifier.
289J	Analog Devices hybrid insolation amplifier. Used to decouple speed signal ground reference points at motor drive, driving cycle generator circuit, and signal conditioning circuits.

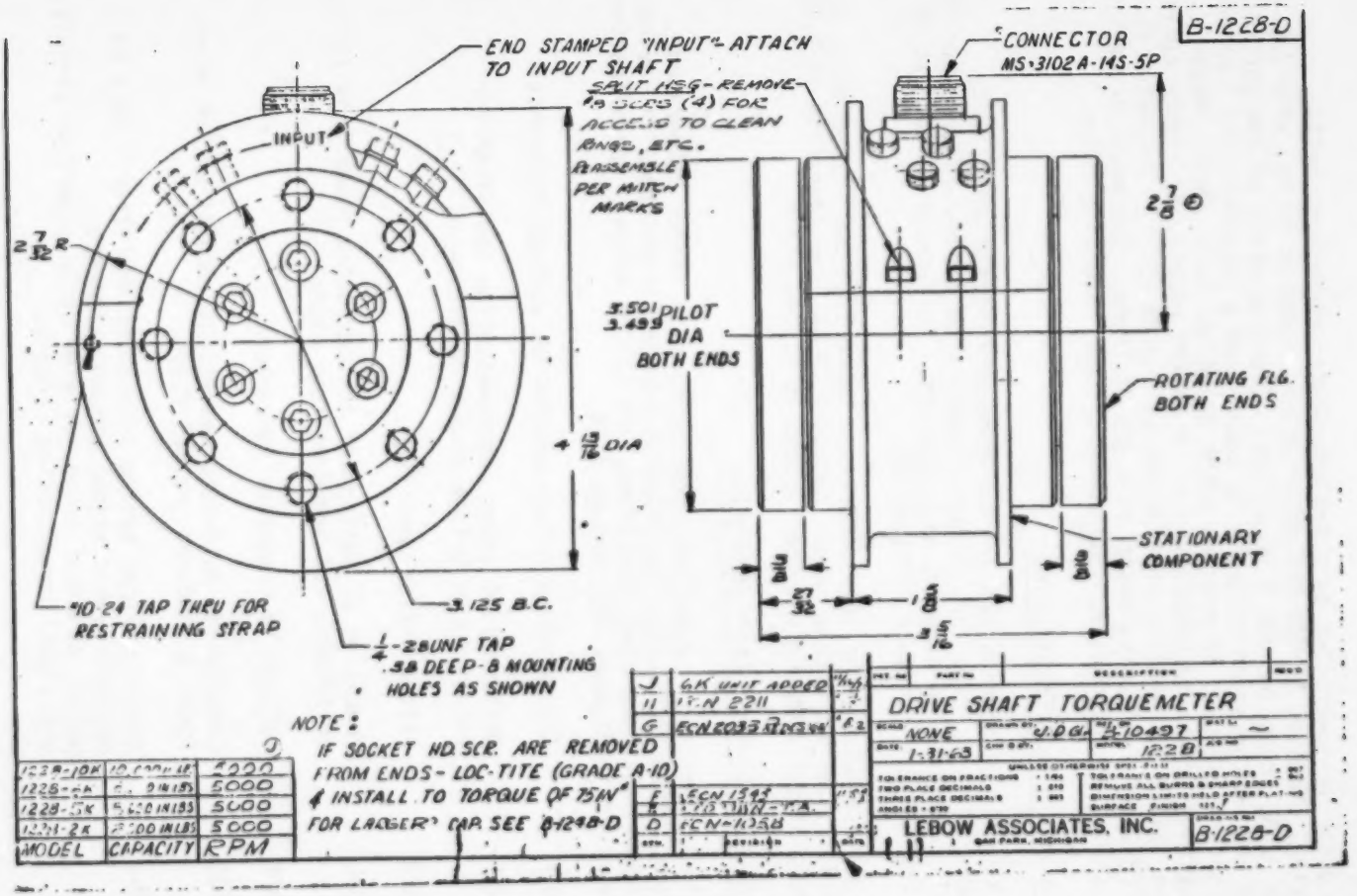
B-1228-D
END STAMPED "INPUT" ATTACH TO INPUT SHAFT
SPLIT HSG - REMOVE #8 SCRS (4) FOR ACCESS TO CLEAN RINGS, ETC. REASSEMBLE PER MATCH MARKS
CONNECTOR MS-3102A-14S-5P
INPUT
2 7/32 R
3.501 3.499 PILOT DIA BOTH ENDS
ROTATING FLG. BOTH ENDS
STATIONARY COMPONENT
4 13/16 DIA
3.125 B.C.
#10-24 TAP THRU FOR RESTRAINING STRAP
1/4-28UNF TAP .38 DEEP-8 MOUNTING HOLES AS SHOWN
NOTE: IF SOCKET HD. SCR. ARE REMOVED FROM ENDS - LOC-TITE (GRADE A-10) & INSTALL TO TORQUE OF 75 IN# FOR LARGER CAP. SEE B-1248-D
MODEL | CAPACITY | RPM
1228-10K | 10,000 IN LBS | 4200
1228-5A | 5,000 IN LBS | 5000
1228-5K | 5,000 IN LBS | 5000
1228-2K | 2,000 IN LBS | 5000
J 6K UNIT ADDED
H E.C.N. 2211
G E.C.N. 2033
F E.C.N. 1595
E 1/8 THK - P.A.
D E.C.N. 1058
DRIVE SHAFT TORQUEMETER
NONE
J.D.G.
1-31-63
A-10497
1228
LEBOW ASSOCIATES, INC.
B-1228-D

Figure A-5. Torque Transducer

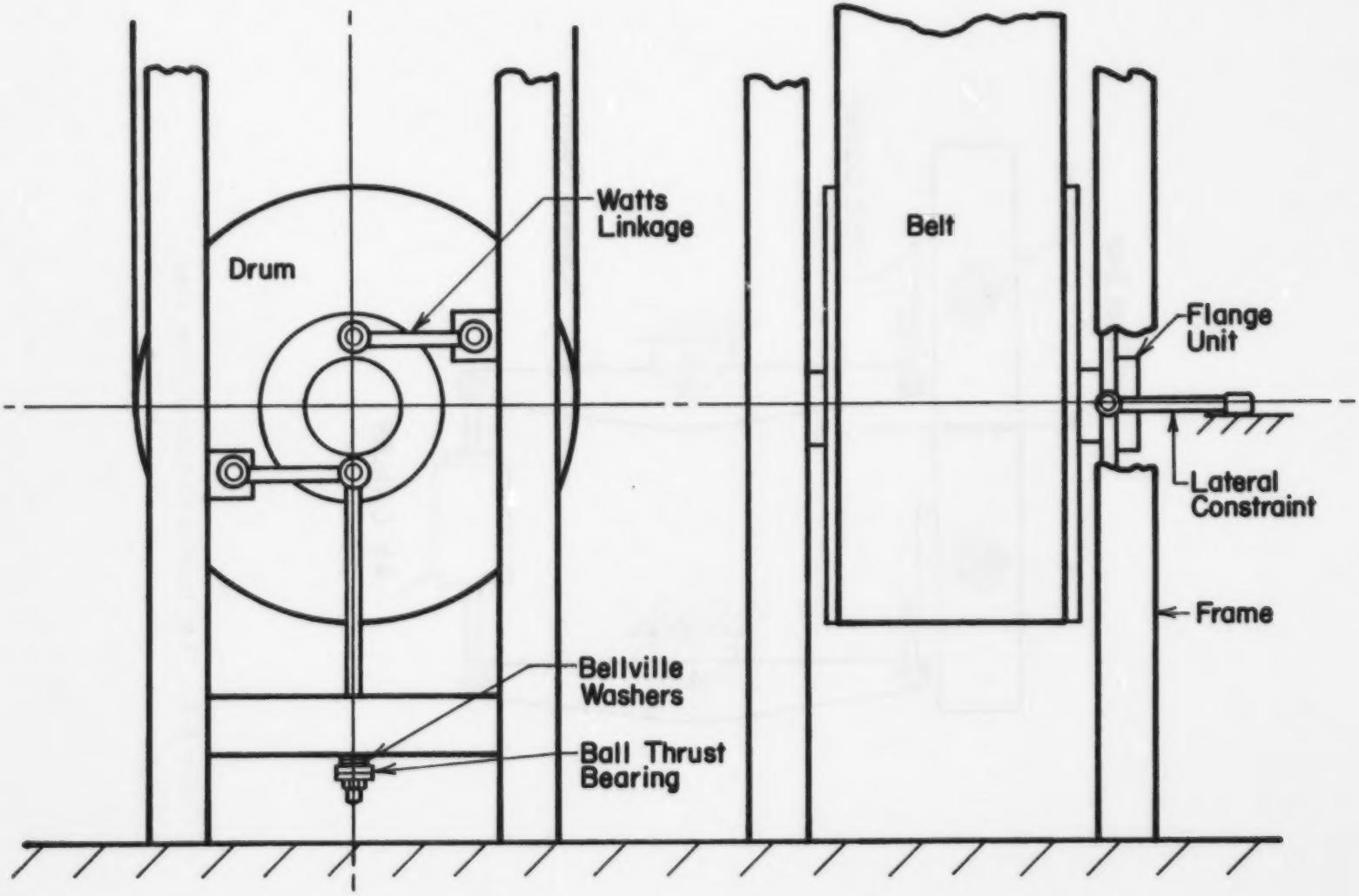

Figure A-6. Lower down location and loading mechanisms

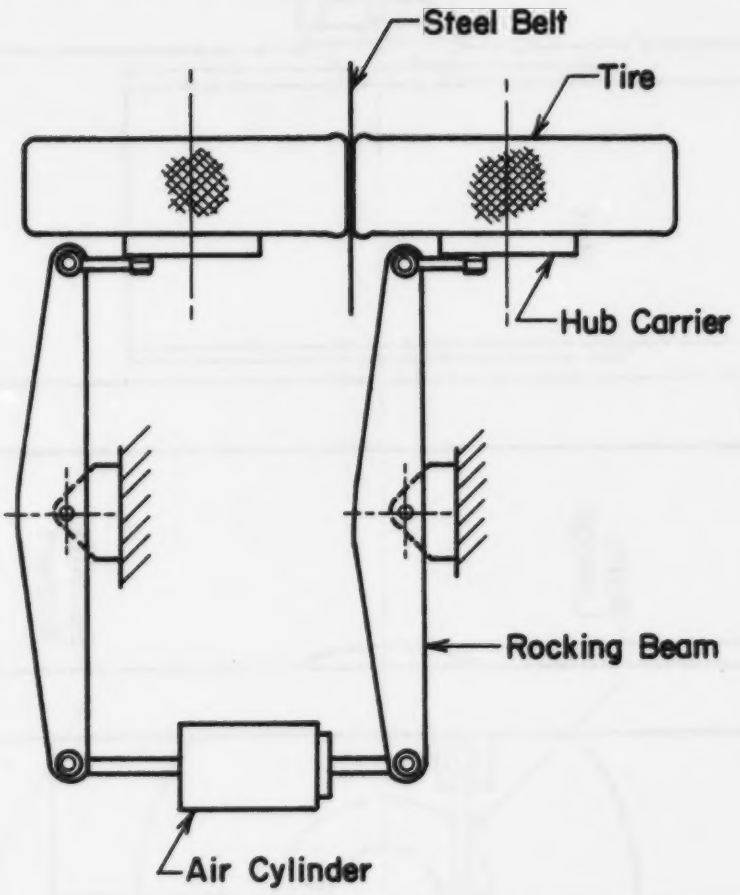

Figure A-7. Tire loading mechanism - top view

SPECIFICATIONS (typical @ V_{IN} = +15V and +25°C unless otherwise noted)

MODEL	AD581J	AD581K	AD581L	AD581S	AD581T	AD581U
ABSOLUTE MAX RATINGS						
Input Voltage V_{IN} to Ground	40V	•	•	•	•	•
Power Dissipation @ +25°C	600mW	•	•	•	•	•
Operating Junction Temp. Range	-55°C to +150°C	•	•	•	•	•
Storage Temperature Range	-65°C to +175°C	•	•	•	•	•
Lead Temperature (Soldering, 10sec)	+300°C	•	•	•	•	•
Thermal Resistance Junction-to-Ambient	150°C/Watt	•	•	•	•	•
Operating Temperature Range	0 to +70°C	•	•	-55°C to +125°C **		**
OUTPUT VOLTAGE TOLERANCE (Error from nominal 10.000V output)	±30mV max	±10mV max	±5mV max	±30mV max	±10mV max	±5mV max
OUTPUT VOLTAGE CHANGE Maximum Deviation from +25°C						
Value T_{min} to T_{max}	±13.5mV	±6.75mV	±2.25mV	±30mV	±15mV	±10mV
(Temperature Coefficient)	(30ppm/°C)	(15ppm/°C)	(5ppm/°C)	(30ppm/°C)	(15ppm/°C)	(10ppm/°C)
LINE REGULATION						
$15V \leq V_{IN} \leq 30V$	3mV max (0.002%/V)	•	•	•	•	•
$13V \leq V_{IN} \leq 15V$	1mV max (0.005%/V)	•	•	•	•	•
LOAD REGULATION $0 \leq I_{OUT} \leq 5mA$	500µV/mA max	•	•	•	•	•
	200µV/mA typ	•	•	•	•	•
QUIESCENT CURRENT	1.0mA max	•	•	•	•	•
	750µA typ	•	•	•	•	•
TURN-ON SETTLING TIME TO 0.1%[1]	200µs	•	•	•	•	•
NOISE (0.1 to 10Hz)	50µV p-p	•	•	•	•	•
LONG-TERM STABILITY	25ppm/1000 Hrs. (Non-Cumulative)	•	•	•	•	•
SHORT CIRCUIT CURRENT	30mA	•	•	•	•	•
OUTPUT CURRENT						
Source @ +25°C	10mA min	•	•	•	•	•
Source T_{min} to T_{max}	5mA min	•	•	•	•	•
Sink T_{min} to T_{max}	5mA min	•	•	200µA min	**	**
Sink -55°C to +85°C	—	—	—	5mA min	**	**
PRICE						
1-24	$4.25	$8.95	$17.95	$14.95	$23.95	$38.75
25-99	$3.45	$7.45	$14.50	$12.50	$20.50	$31.50
100-999	$2.85	$5.95	$11.95	$ 9.95	$15.95	$25.75
				AD581S/883B	AD581T/883B	AD581U/883B
1-24	The AD581S, T and U are available with full processing to MIL-STD-883A Class B. A complete list of procedures is available on request.			$18.95	$27.95	$45.00
25-99				$15.50	$23.50	$37.50
100-999				$12.50	$18.50	$30.00

*Specifications same as AD581J.
**Specifications same as AD581S.
[1] See Figure 8.
Specifications and prices subject to change without notice.

Figure A-8. AD581 Precision Voltage Reference

SPECIFICATIONS (typical @ V_S = ±15V, R_L = 2kΩ and T_A = 25°C unless otherwise specified)

MODEL	AD521J	AD521K	AD521S
GAIN			
Range (For Specified Operation. Note 1.)	1 to 1000	"	"
Equation	$G = R_S/R_G$ V/V	"	"
Error from Equation	(±0.25–0.004G)%	"	"
Nonlinearity (Note 2)			
1≤G≤1000	0.2% max	"	"
Gain Temperature Coefficient	±(3 ±0.05G)ppm/°C	"	±(15 ±0.4G)ppm/°C
OUTPUT CHARACTERISTICS			
Rated Output	±10V, ±10mA min	"	"
Output at Maximum Operating Temperature	±10V @ 5mA min	"	"
Impedance	0.1Ω	"	"
DYNAMIC RESPONSE			
Small Signal Bandwidth (-3dB)			
G = 1	>2MHz	"	"
G = 10	300kHz	"	"
G = 100	200kHz	"	"
G = 1000	40kHz	"	"
Small Signal, ±1.0% Flatness			
G = 1	75kHz	"	"
G = 10	26kHz	"	"
G = 100	24kHz	"	"
G = 1000	6kHz	"	"
Full Peak Response (Note 3)	100kHz	"	"
Slew Rate, 1≤G≤1000	10V/μsec	"	"
Settling Time (any 10V step to within 10mV of Final Value)			
G = 1	7μsec	"	"
G = 10	5μsec	"	"
G = 100	10μsec	"	"
G = 1000	33μsec	"	"
Differential Overload Recovery (±30V input to within 10mV of Final Value) (Note 4)			
G = 1000	50μsec	"	"
Common Mode Step Recovery (10V input to within 10mV of Final Value) (Note 5)			
G = 1000	10μsec	"	"
VOLTAGE OFFSET (may be nulled)			
Input Offset Voltage (V_{OS_I})	3mV max (2mV typ)	1.5mV max (0.5mV typ)	**
vs. Temperature	15μV/°C max (7μV/°C typ)	5μV/°C max (1.5μV/°C typ)	**
vs. Supply	3μV/%	"	"
Output Offset Voltage (V_{OS_O})	400mV max (200mV typ)	200mV max (30mV typ)	**
vs. Temperature	400μV/°C max (150μV/°C typ)	150μV/°C max (50μV/°C typ)	**
vs. Supply (Note 6)	0.005V_{OS_I}/%	"	"
INPUT CURRENTS			
Input Bias Current (either input)	50nA max	40nA max	**
vs. Temperature	1nA/°C max	500pA/°C max	**
vs. Supply	2%/V	"	"
Input Offset Current	20nA max	10nA max	**
vs. Temperature	250pA/°C max	125pA/°C max	**
INPUT			
Differential Input Impedance (Note 7)	3 x 10⁸Ω‖1.8pF	"	"
Common Mode Input Impedance (Note 8)	6 x 10¹⁰Ω‖3.0pF	"	"
Input Voltage Range for Specified Performance	±10V	"	"
Maximum Voltage without Damage to Unit, Power ON or OFF Differential Mode (Note 9)	30V	"	"
Voltage at either input (Note 10)	V_S ±15V	"	"
Common Mode Rejection Ratio, DC to 60Hz with 1kΩ source unbalance			
G = 1	70dB min (74dB typ)	74dB min (80dB typ)	**
G = 10	90dB min (94dB typ)	94dB min (100dB typ)	**
G = 1000	100dB min (104dB typ)	104dB min (114dB typ)	**
G = 1000	100dB min (110dB typ)	110dB min (120dB typ)	**
NOISE			
Voltage RTO (p-p) @ 0.1Hz to 10Hz (Note 10)	$\sqrt{(10.5G)^2 + (225)^2}$ μV	"	"
RMS RTO, 10Hz to 10kHz	$\sqrt{(1.2G)^2 + (50)^2}$ μV	"	"
Input Current, rms, 10Hz to 10kHz	15pA (rms)	"	"
REFERENCE TERMINAL			
Bias Current	1μA	"	"
Input Resistance	10MΩ	"	"
Voltage Range	±10V	"	"
Gain to Output	1	"	"
POWER SUPPLY			
Operating Voltage Range	±5 to ±18	"	"
Quiescent Supply Current	5mA max	"	"
TEMPERATURE RANGE			
Specified Performance	0 to +70°C	"	-55 to +125°C
Operating	-25 to +85°C	"	-55 to +125°C
Storage	-65 to +150°C	"	"
PRICE			
(1-24)	$12.75	$18.00	$30.00
(25-99)	$10.20	$14.40	$24.00
(100-999)	$8.50	$12.00	$20.00

*Specification same as AD521J.
**Specification same as AD521K.

Specifications and prices subject to change without notice.

Figure A-9. AD521 Instrumentation Amplifier

SPECIFICATIONS (typical @ +25°C and ±15V dc unless otherwise noted)

MODEL	AD517J	AD517K	AD517L	AD517S[1]
OPEN LOOP GAIN				
V_O = ±10V, $R_L \geq 2k\Omega$	10^6 min	•	•	•
T_{min} to T_{max}	500,000 min	•	•	250,000
OUTPUT CHARACTERISTICS				
Voltage @ $R_L \geq 2k\Omega$, T_{min} to T_{max}	±10V min	•	•	•
Load Capacitance	1000pF	•	•	•
Output Current	10mA min	•	•	•
Short Circuit Current	25mA	•	•	•
FREQUENCY RESPONSE				
Unity Gain, Small Signal	250kHz	•	•	•
Full Power Response	1.5kHz	•	•	•
Slew Rate, Unity Gain	0.10V/μs	•	•	•
INPUT OFFSET VOLTAGE				
Initial Offset, $R_S \leq 10k\Omega$	150μV max	50μV max	25μV max	••
vs. Temp., T_{min} to T_{max}	3.0μV/°C max	1.0μV/°C max	0.5μV/°C max	••
vs. Supply	25μV/V max	10μV/V max	••	••
(T_{min} to T_{max})	40μV/V max	15μV/V max	••	20μV/V max
INPUT OFFSET CURRENT				
Initial	1nA max	0.75nA max	0.25nA max	••
T_{min} to T_{max}	1.5nA max	1.25nA max	0.4nA max	2nA max
INPUT BIAS CURRENT				
Initial	5nA max	2nA max	1nA max	••
T_{min} to T_{max}	8nA max	3.5nA max	1.5nA max	10nA max
vs. Temp, T_{min} to T_{max}	±20pA/°C	±10pA/°C	±4pA/°C	••
INPUT IMPEDANCE				
Differential	15MΩ‖1.5pF	20MΩ‖1.5pF	••	••
Common Mode	$2.0 \times 10^{11}\ \Omega$	•	•	•
INPUT NOISE				
Voltage, 0.1Hz to 10Hz	2μV p-p	•	•	•
f = 10Hz	35nV/√Hz	•	•	•
f = 100Hz	25nV/√Hz	•	•	•
f = 1kHz	20nV/√Hz	•	•	•
Current, f = 10Hz	0.05pA/√Hz	•	•	•
f = 100Hz	0.03pA/√Hz	•	•	•
f = 1kHz	0.03pA/√Hz	•	•	•
INPUT VOLTAGE RANGE				
Differential or Common Mode max Safe	$\pm V_S$	•	•	•
Common Mode Rejection, V_{in} = ±10V	94dB min	110dB min	••	••
Common Mode Rejection, T_{min} to T_{max}	94dB min	100dB min	••	••
POWER SUPPLY				
Rated Performance	±15V	•	•	•
Operating	±(5 to 18)V	•	•	±(5 to 22)V
Current, Quiescent	4mA max	3mA max	••	••
TEMPERATURE RANGE				
Operating Rated Performance	0 to +70°C	•	•	-55°C to +125°C
Storage	-65°C to +150°C	•	•	•
PRICES				
(1–24)	$6.75	$11.25	$18.75	$27.00
(25–99)	$5.50	$ 9.50	$15.50	$22.50
(100–999)	$4.50	$ 7.50	$12.50	$18.00

NOTES
*Specifications same as AD517J
**Specifications same as AD517K
Specifications subject to change without notice.
[1] The AD517S is available fully processed and screened to the requirements of MIL-STD-883A, Level B. Consult factory for pricing.

Figure A-10. AD517 Precision Operational Amplifier

SPECIFICATIONS (typical at +25°C, with $\pm V_S$ = 15V, $R_L > 2k$, unless otherwise stated)

PARAMETER	CONDITIONS	AD534J	AD534K	AD534L	AD534S	AD534T
MULTIPLIER PERFORMANCE						
Transfer Function		$\frac{(X_1 - X_2)(Y_1 - Y_2)}{10} + Z_2$	*	*	*	*
Total Error[1]	$-10V \leq X, Y \leq +10V$	±1.0% max	±0.5% max	±0.25% max	*	**
	T_A = min to max					
	V_S = ±14 to ±16V	±1.5%	±1.0%	±0.5%	±2.0% max	±1.0% max
vs. Temperature		±0.022%/°C	±0.015%/°C	±0.008%/°C	±0.02%/°C max	±0.01%/°C max
Scaling Voltage Error	SF = 10.00 nominal[2]	±0.25%	±0.1%	**	*	**
Temperature-Coefficient of Scaling-Voltage	T_A = min to max	±0.02%/°C	±0.01%/°C	±0.005%/°C	*	±0.005%/°C max
Supply-Related Error	$\pm V_S$ = (15V) ±1V	±0.01%	*	*	*	*
Nonlinearity, X	X = 20V pk-pk Y = ±10V	±0.4%	±0.2% (0.3% max)	±0.1% (0.12% max)	*	**
Nonlinearity, Y	Y = 20V pk-pk X = ±10V	±0.01%	±0.01% (±0.1% max)	±0.005% (±0.1% max)	*	**
Feedthrough[3], X	X = 20V pk-pk 50Hz Y nulled	±0.3%	±0.15% (0.3% max)	±0.05% (0.12% max)	*	**
Feedthrough[3], Y	X nulled Y = 20V pk-pk 50Hz	±0.01%	±0.01% (±0.1% max)	±0.003% (±0.1% max)	*	**
DIVIDER PERFORMANCE						
Transfer Function	$X_1 > X_2$	$10\frac{(Z_2 - Z_1)}{(X_1 - X_2)} + Y_1$	*	*	*	*
Total Error[1]	X = 10V $-10V \leq Z \leq +10V$	±0.75%	±0.35%	±0.2%	*	**
	X = 1V $-1V \leq Z \leq +1V$	±2.0%	±1.0%	±0.8%	*	**
(Note 4)	$0.1V \leq X \leq 10V$ $-10V \leq Z \leq +10V$	±2.5%	±1.0%	±0.8%	*	**
SQUARER PERFORMANCE						
Transfer Function		$\frac{(X_1 - X_2)^2}{10} + Z_2$	*	*	*	*
Total Error[1]	$-10V \leq X \leq +10V$	±0.6%	±0.3%	±0.2%	*	**
SQUARE-ROOTER PERFORMANCE						
Transfer Function	$Z_1 > Z_2$	$\sqrt{10(Z_2 - Z_1)} + X_2$	*	*	*	*
Total Error[1]	$1V \leq Z \leq 10V$	±1.0%	±0.5%	±0.25%	*	**
INPUT AMPLIFIERS (X, Y and Z)[5]						
Signal Voltage Range	Rated Accuracy (Diff. or CMR)	±10V	*	*	*	*
	Operating (Diff.)	±12V	*	*	*	*
Offset Voltage, X, Y		±5mV (±20mV max)	±2mV (±10mV max)	**	*	**
Drift	T_A = min to max	100µV/°C	50µV/°C	**	*	150µV/°C
Offset Voltage, Z		±5mV (±30mV max)	±2mV (±15mV max)	±2mV (±10mV max)	*	**
Drift	T_A = min to max	200µV/°C	100µV/°C	**	500µV/°C max	300µV/°C max
CMRR (X, Y, Z)	50Hz, 20V pk-pk	80dB (60dB min)	90dB (70dB min)	**	*	**
Bias Current	Diff. Input = 0	0.8µA (2µA max)	*	*	*	*
Offset Current	Diff. Input = 0	0.1µA	*	0.05µA (0.2µA max)	*	*
Differential Resistance		10MΩ	*	*	*	*
OUTPUT AMPLIFIER[5]						
Open-Loop Gain	f = 50Hz	70dB	*	*	*	*
Small-Signal BW	V_{OUT} = 0.1V rms	1MHz	*	*	*	*
1% Amplitude Error	C_{LOAD} = 1000pF	50kHz	*	*	*	*
Output Voltage Swing	T_A = min to max	±11V min	*	*	*	*
Slew Rate	V_{OUT} 20V pk-pk	20V/µs	*	*	*	*
Settling Time to ±1%	ΔV_{OUT} = 20V	2µs	*	*	*	*
Output Impedance	Unity-Gain, f ≤1kHz	0.1Ω	*	*	*	*
Noise Spectral-Density	SF = 10	$0.8\mu V/\sqrt{Hz}$	*	*	*	*
	SF = 3 (Note 6)	$0.4\mu V/\sqrt{Hz}$	*	*	*	*
Wideband Noise	f = 10Hz to 5MHz	1mV rms	*	*	*	*
	f = 10Hz to 10kHz	90µV rms	*	*	*	*
	f = 10Hz to 10kHz, SF = 3 (Note 6)	60µV rms	*	*	*	*
Maximum Output Current	R_L = 0, T_A = min to max	30mA	*	*	*	*
POWER SUPPLY SPECIFICATIONS						
Supply Voltage	Rated Performance	±15V	*	*	*	*
	Operating	±8 to ±18V	*	*	±8 to ±22V	±8 to ±22V
Supply Current	Quiescent	4mA (6mA max)	*	*	*	*
PRICES	(1–24)	$26.00	$36.00	$55.00	$68.00	$90.00
	(25–99)	$21.00	$30.00	$45.00	$56.00	$75.00
	(100–999)	$16.00	$24.00	$36.00	$45.00	$60.00

NOTES
*Same as AD534J spec. **Same as AD534K spec.
Specifications subject to change without notice.

[1] Figures given are percent of full-scale, ±10V (i.e., 0.01% = 1mV).
[2] May be reduced down to 1V using external resistor between $-V_S$ and SF.
[3] Irreducible component due to nonlinearity; excludes effect of offsets.
[4] With external Z-offset adjustment, $Z \leq \pm X$.
[5] See Functional Block Diagram, Figure 1, for definitions of sections.
[6] Using external resistor adjusted to give SF = 3.

Figure A-11. AD534 Precision Analog Multiplier

SPECIFICATIONS (typical @ +25°C with V_S (total) = 5 to 36V, unless otherwise noted)

MODEL	AD537J	AD537K	AD537S	
ANALOG INPUT AMPLIFIER				
(Voltage-to-Current Converter)				
Voltage Input Range				
Single Supply	0 to ($+V_S$ - 4) Volts (min)	*	*	
Dual Supply	$-V_S$ to ($+V_S$ - 4) Volts (min)	*	*	
Input Bias Current				
(Either Input)	100nA	*	*	
Input Resistance (Non-Inverting)	250MΩ	*	*	
Input Offset Voltage				
(Trimmable to Zero)	5mV max	2mV max	**	
vs. Supply	100μV/V max	*	*	
vs. Temp (T_{min} to T_{max})	5μV/°C	1μV/°C	10μV/°C max	
Safe Input Voltage (Note 1)	$\pm V_S$	*	*	
CURRENT-TO-FREQUENCY CONVERTER				
Frequency Range	0 to 150kHz	*	*	
Nonlinearity (Note 2)				
f_{max} = 10kHz	0.13% max (0.1% typ)	0.07% max	**	
f_{max} = 100kHz	0.25% max (0.15% typ)	0.1% max	**	
Full Scale Calibration Error				
C = 0.0100μF, I_{IN} = 1.000mA	±7% max	±5% max	**	
vs. Supply, ($f_{max} \leq$ 100kHz)	±0.1%/V max (0.01% typ)	*	*	
vs. Temp. (T_{min} to T_{max})	±150ppm/°C max (50ppm typ)	50ppm/°C max (30ppm typ)	150ppm/°C max	
REFERENCE OUTPUTS				
Voltage Reference				
Absolute Value	1.00 Volt ±5% max	*	*	
vs. Temp. (T_{min} to T_{max})	50ppm/°C	100ppm/°C max	**	
vs. Supply	±0.05%/V max	*	*	
Output Resistance (Note 4)	380Ω	*	*	
Absolute Temperature Reference (Note 3)				
Nominal Output Level	1.00mV/°K	*	*	
Initial Calibration @ +25°C	298mV ±5mV typ	±5mV max	**	
Slope Error from 1.00mV/°K	±0.02mV/°K	*	*	
Slope Nonlinearity	±0.1°K	*	*	
Output Resistance (Note 4)	900Ω	*	*	
OUTPUT INTERFACE (Open Collector Output)				
(Symmetrical Square Wave)				
Output Sink Current in Logic "0"				
(V_{OUT} = 0.4V max, T_{min} to T_{max})	20mA min	*	10mA min	
Output Leakage Current in Logic "1"				
(T_{min} to T_{max})	200nA max	*	2μA max	
Logic Common Level Range	$-V_S$ to ($+V_S$ - 4) Volts	*	*	
Rise/Fall Times (C_T = 0.01μF)				
I_{IN} = 1mA	0.2μs	*	*	
I_{IN} = 1μA	1μs	*	*	
POWER SUPPLY				
Voltage, Rated Performance				
Single Supply	4.5 to 36V	*	*	
Dual Supply	±5 to ±18V	*	*	
Quiescent Current	1.2mA	*	*	
TEMPERATURE RANGE				
Rated Performance	0 to +70°C	*	-55°C to +125°C	
Storage	-65°C to +150°C	*	*	
PRICE				AD5375/883B (Note 5)
(1-24)	$13.00	$20.00	$29.00	$36.00
(25-99)	$11.50	$16.00	$23.00	$29.00
(100-999)	$ 9.50	$13.50	$19.00	$24.00

*Specifications same as AD537J.
**Specifications same as AD537K.

Specifications subject to change without notice.

Note 1 Maximum voltage input level is equal to the supply on either input terminal. However, large negative voltage levels can be sensed at the negative terminal if the input is scaled to a nominal 1mA full scale through an appropriate value resistor. (See Figure 3)

Note 2 Nonlinearity is specified for a current input level (I_{IN}) to the converter from 0.1 to 1000μA. Converter has 100% overrange capability up to I_{IN} = 2000μA with slightly reduced linearity. Nonlinearity is defined as deviation from a straight line from zero to full scale, expressed as a percentage of full scale.

Note 3 Temperature reference output performance is specified from 0 to +70°C for "J" and "K" devices, -55°C to +125°C for "S" model.

Note 4 Loading the 1.0 volt or 1mV/°K outputs can cause a significant change in overall circuit performance, as indicated in the applications section on page 4. To maintain normal operation, these outputs should be operated into the internal buffer or an external amplifier.

Note 5 The AD5375/883B is an AD5375 which is inspected and processed to the full requirements of MIL-STD-883A, Level B. A complete listing of the tests is available on request.

Figure A-12. AD537 Voltage To Frequency Converter

The instrumentation for each transducer is referenced to a ground point on the transducer and decoupled from all other ground points.

To eliminate spurious interrupts, the microcomputer interrupt lines are buffered with the circuit shown in Figure A-15.

OPERATING CHARACTERISTICS:

Test Conditions: $V^+ = +5$ volts, $V^- = -5$ volts, $T_A = +25°C$, DR pin connected to V^+ ($f_{COM} \approx 160Hz$), $C_1 = C_2 = 1\mu F$, Test Circuit 1, unless otherwise specified.

PARAMETER	SYMBOL	CONDITIONS		MIN	VALUE TYP	MAX	UNIT
Input Offset Voltage	V_{OS}	$R_S \leq 1k\Omega$	Low Bias Setting		±2		µV
		$C_1 = C_2 = 1\mu F$	Med Bias Setting		±2	±5	µV
			High Bias Setting		±7		µV
		MIL version over temp.	Med Bias Setting			±20	µV
Long Term Input Offset Voltage Stability	$V_{OS/Time}$	Low or Med Bias Settings			0.2		µV/year
Average Input Offset Voltage Temperature Coefficient	TCVos	Low or Med Bias Settings	$-55°C > T_A > +25°C$		0.005	0.1	µV/°C
			$+25°C > T_A > +85°C$		0.01	0.1	µV/°C
			$+25°C > T_A > +125°C$		0.05	0.15	µV/°C
Noise Voltage (RMS)	e_n	Band Width	Low Bias		0.8		µV
		0.1 to 10Hz	Med Bias		0.8		µV
		$R_S \leq 1k\Omega$	High Bias		1.0		µV
Equivalent Input Noise Voltage Peak-to-peak	e_{np-p}	Band Width	Low Bias		4.0		µV
		0.1 to 10Hz	Med Bias		4.0		µV
		$R_S \leq 1k\Omega$	High Bias		5.0		µV
Spot equivalent Noise voltage	e_{n10}	f = 10Hz Band Width 1Hz				700	nV/√Hz
Spot equivalent Noise Current	i_{n10}	f = 10Hz Band Width 1Hz				0.1	pA/√Hz
Differential Input Voltage Range	DIF V_{IN}			V^--0.3	to	V^++0.3	V
Common Mode Input Range	CMVR	Low Bias		-4.2		+4.2	V
		Med Bias		-4.0		+4.0	V
		High Bias		-3.5		+3.5	V
Common Mode Rejection Ratio	CMRR	Any Bias Setting			88		dB
Power Supply Rejection Ratio	PSRR	Any Bias Setting			110		dB
Non Inverting Input Bias Current	I_{INB}	Any Bias Setting, (Includes charge injection currents)			0.300	3	nA
Inverting Input Bias Current	I_{IB}	Any Bias Setting, (Includes charge injection currents)			0.150	1.5	nA
Voltage Gain	A_V	$R_L = 100k\Omega$	Low Bias	90	105		dB
			Med Bias	90	105		dB
			High Bias	80	100		dB
Maximum Output Voltage Swing	V_{OUT}	$R_L = 1M\Omega$			±4.9		V
							V
		$R_L = 100k\Omega$			±4.8		V
							V
		$R_L = 10k\Omega$	Positive Swing	+4.4			V
			Negative Swing			-4.5	V
Large Signal Slew Rate	SR	Unity	High Bias Setting		1.8		V/µs
		Gain	Med Bias Setting		0.5		V/µs
		ICL7600	Low Bias Setting		0.2		V/µs
Unity Gain Band Width	GBW		High Bias Setting		1.2		MHz
		ICL7600	Med Bias Setting		0.3		MHz
		Test Circuit 2	Low Bias Setting		0.12		MHz
Extrapolated Unity Gain Band Width	GBW		High Bias Setting		1.8		MHz
		ICL7601	Med Bias Setting		0.4		MHz
			Low Bias Setting		0.2		MHz
BIAS Terminal Input Current	I_{BIAS}	V^--0.3 ≤ V_{BIAS} ≤ V^++0.3 volt			±30		pA
BIAS Voltage to Define Current Modes	V_{BH}	Low Bias Setting		V^+ 0.3		V^++0.3	V
	V_{BM}	Med Bias Setting		V^-+1.4		V^+-1.4	V
	V_{BL}	High Bias Setting		V^--0.3		V^++0.3	V
DR (Division Ratio) Input Current	I_{DR}	V^+-8.0V ≤ V_{DR} ≤ V^++0.3V			±30		pA
DR Voltage to define oscillator division ratio	V_{DRH}	Internal oscillator division ratio 32		V^+-0.3		V^++0.3	V
	V_{DRL}	Internal oscillator division ratio 2		V^+-8		V^-+1.4	V
Nominal Commutation Frequency	f_{COM}	Cosc = 0 pF	DR Connected to V^+		160		Hz
			DR Connected to GND		2560		Hz
Supply Current	I_S	High Bias Setting		4	7	15	mA
		Medium Bias Setting		0.6	1.7	5	mA
		Low Bias Setting		0.25	0.6	1.5	mA
Operating Supply Voltage Range	V^+ V	High Bias Setting		5		16	V
		Medium or Low Bias Setting		4		16	V

Figure A-13. ICL7601 (now AM 7601) Commutating Auto-Zero Operational Amplifier

SPECIFICATIONS (typical @ +25°C and V_S = +14.4V to +25V dc unless otherwise noted.)

Model	289J	289K	289L
GAIN (NONINVERTING)			
Range		1 to 1000V/V	
Formula		$G = 1 + \frac{10k\Omega}{R_G(k\Omega)}$	
Deviation from Formula		±1.5% max	
vs. Temperature (0 to +70°C)[1]		15ppm/°C typ (50ppm/°C max)	
Nonlinearity, (±5V Swing)[1,2]	±0.05% max	±0.025% max	±0.012% max
INPUT VOLTAGE RATINGS			
Linear Differential Range (G = 1V/V)		±10V min	
Max Safe Differential Input			
Continuous		120V rms	
1 Minute		240V rms	
Max CMV (Inputs to Outputs)			
Continuous ac or dc		±2500V peak max	
ac, 60Hz, 1 Minute Duration		2500V rms	
CMR, Inputs to Outputs 60Hz			
$R_S \leq 1k\Omega$, Balanced Source Impedance		120dB	
$R_S \leq 1k\Omega$, HI IN Lead Only		104dB min	
Max Leakage Current, Input to Output @ 115V rms, 60Hz ac		2µA rms max	
INPUT IMPEDANCE			
Differential		$3pF \| 10^9\Omega$	
Overload		100kΩ	
Common Mode		$20pF \| 5 \times 10^{10}\Omega$	
INPUT DIFFERENCE CURRENT			
Initial @ +25°C		10nA (75nA max)	
vs. Temperature (0 to 70°C)		0.15nA/°C	
INPUT NOISE (GAIN = 100V/V)			
Voltage			
0.05Hz to 100Hz		8µV p-p	
10Hz to 1kHz		3µV rms	
Current			
0.05Hz to 100Hz		3pA rms	
FREQUENCY RESPONSE			
Small Signal -3dB			
G = 1V/V		20kHz	
G = 100V/V		5kHz	
Full Power, 10V p-p Output			
G = 1V/V		5kHz	
G = 100V/V		3.5kHz	
Full Power, 20V p-p Output			
G = 1V/V		2.3kHz	
G = 100V/V		2.3kHz	
Slew Rate		0.14V/µs	
OFFSET VOLTAGE, REFERRED TO INPUT			
Initial, @ +25°C		$\pm 3 \pm \frac{10}{G}$ mV max	
vs. Temperature (0 to +70°C)	$\pm 20 \pm \frac{200}{G}$ max	$\pm 15 \pm \frac{100}{G}$ max	$\pm 10 \pm \frac{50}{G}$ µV/°C max
vs. Supply Voltage (+15V to +20V change)		$\pm 2 \pm \frac{10}{G}$ µV/V	
RATED OUTPUT			
Voltage, 2kΩ Load		±10V min	
Output Impedance		<1Ω(dc to 100Hz)	
Output Ripple, 0.1MHz Bandwidth			
No Signal IN		5mV p-p	
$+10V_{IN}$		50mV p-p	
ISOLATED POWER SUPPLY			
Voltage		±15V dc	
Accuracy		±10%	
Current		±5mA, min	
Regulation No Load to Full Load		±5%	
Ripple, 0.1MHz Bandwidth, No Load		25mV p-p	
Full Load		75mV p-p	
POWER SUPPLY, SINGLE POLARITY[4]			
Voltage, Rated Performance		+14.4V to +25V	
Voltage, Operating		+8.5V to +25V	
Current, Quiescent (@ V_S = +15V)		+23mA	
TEMPERATURE RANGE			
Rated Performance		0 to +70°C	
Operating		-15°C to +75°C	
Storage		-55°C to +85°C	
CASE DIMENSIONS		1.5" X 2.0" X 0.75"	
PRICE			
(1–9)	$39	$69	$99
(10–24)	$49	$59	$89

NOTES:
[1] Gain temperature drift is specified as a percentage of output signal level.
[2] Gain nonlinearity is specified as a percentage of 10V p-p output span.
[3] When isolated power output is used, nonlinearity increases by +0.002%/mA of current drawn.
[4] Recommended power supply, ADI model 900, ±15V @ 50mA output.
Specifications subject to change without notice.

OUTLINE DIMENSIONS

Dimensions shown in inches and (mm).

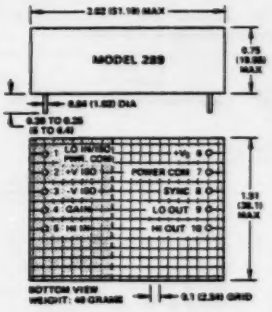

SHIELDED MATING SOCKET
AC1214 $14.50 (1–24)

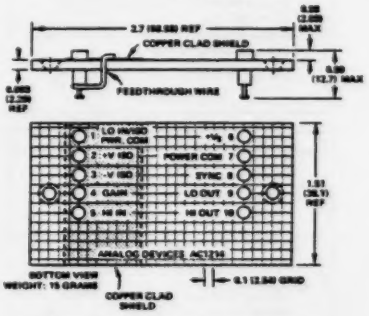

INTERCONNECTIONS AND SHIELDING TECHNIQUE

To preserve the high CMR performance of model 289, care must be taken to keep the capacitance balanced about the input terminals. A shield should be provided on the printed circuit board under model 289 as illustrated in the outline drawing above (screened area). The LO IN/ISO PWR COM (pin 1) must be connected to this shield. This shield is provided with the mounting socket, model AC1214 (solder feedthrough wire to the socket pin 1 and copper foil surface). A recommended shielding technique using model AC1214 is illustrated in Figure 1.

Best CMR performance will be achieved by using twisted, shielded cable for the input signal to reduce inductive and capacitive pickup. To further reduce effective cable capacitance, the cable shield should be connected to the common mode signal source as close to signal low as possible (see Figure 1).

Figure A-14. Analog Devices Model 289 Precision Hybrid Isolation Amplifier

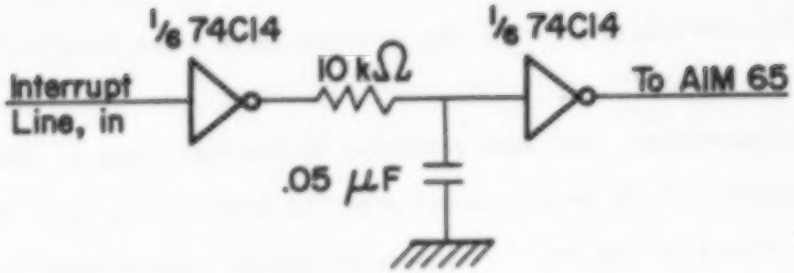

Figure A-15. Interrupt Line Buffer Circuit

APPENDIX B

MOVEMENT OF THE CENTER OF TIRE CONTACT PRESSURE WITH DRIVING AND BRAKING FORCES

B.1 Introduction

When a tire is freely rolling, with no driving or braking torque applied at the axle, a torque balance completely defines the system of forces acting on the tire. Under these conditions, the rolling resistance force generated by the tire, acting about the axle, is balanced by a longitudinal offset of the point of application of the vertical force. The two moments, rolling resistance force times loaded radius and vertical force times longitudinal offset, are equal in magnitude and the latter can rightly be called the rolling resistance moment. But when a driving or braking torque is applied, the angular velocity of the wheel changes from its free rolling value because of the elastic nature of the tire. A power, or energy, balance must now be introduced if the forces acting on the tire are to be completely defined. In consequence, the vertical force times longitudinal offset moment does not express the energy loss characteristics of the tire alone, and cannot legitimately be called the rolling resistance moment. A qualitative explanation of this can be given by considering a tire which is assumed to have no internal energy losses and no losses due to sliding in the contact patch, and is transmitting a driving torque. The power flow into the tire (input torque times angular velocity) is equal to the power flow out of the tire (driving force times forward speed). But, since the driving slip causes angular velocity to be higher than predicted from forward speed and tire radius, the input torque is lower than would be predicted from driving force and tire radius. A longitudinal shift in the position of the vertical force must therefore occur to balance the torques acting across the tire, even though the energy loss in the tire is zero.

B.2 Torque and Power Balances

Figure B-1 shows the forces and moments acting on a tire which is transmitting a driving or braking torque. Camber angle and side force are assumed to be zero. The figure also defines the positive direction of application of the forces and moments, and the positive direction of the tire velocities, as used in the following derivations.

Taking moments about the center of the tire gives the torque equation:

$$T - Z \cdot e - X \cdot R_\ell = 0$$

and

$$Z \cdot e = T - X \cdot R_\ell \qquad \text{(B-1)}$$

where :

T = input torque (driving positive)

Z = vertical load

X = longitudinal force acting on the tire (driving positive)

e = longitudinal offset of the vertical force from a vertical axis through the center of the tire

R_ℓ = loaded radius of the tire

The equation describing power (or energy) flow in a tire can be written down in a number of ways [2,3]. In the present case, however, it is convenient to identify four separate components of the power flowing into and out of the tire.

$T \cdot \omega$ = power flow through the drive axle
= power source in driving and power sink in braking

$X \cdot U$ = useful power at the tire/pavement interface
= sink in driving and source in braking

P_I = internal power loss in the tire
= sink

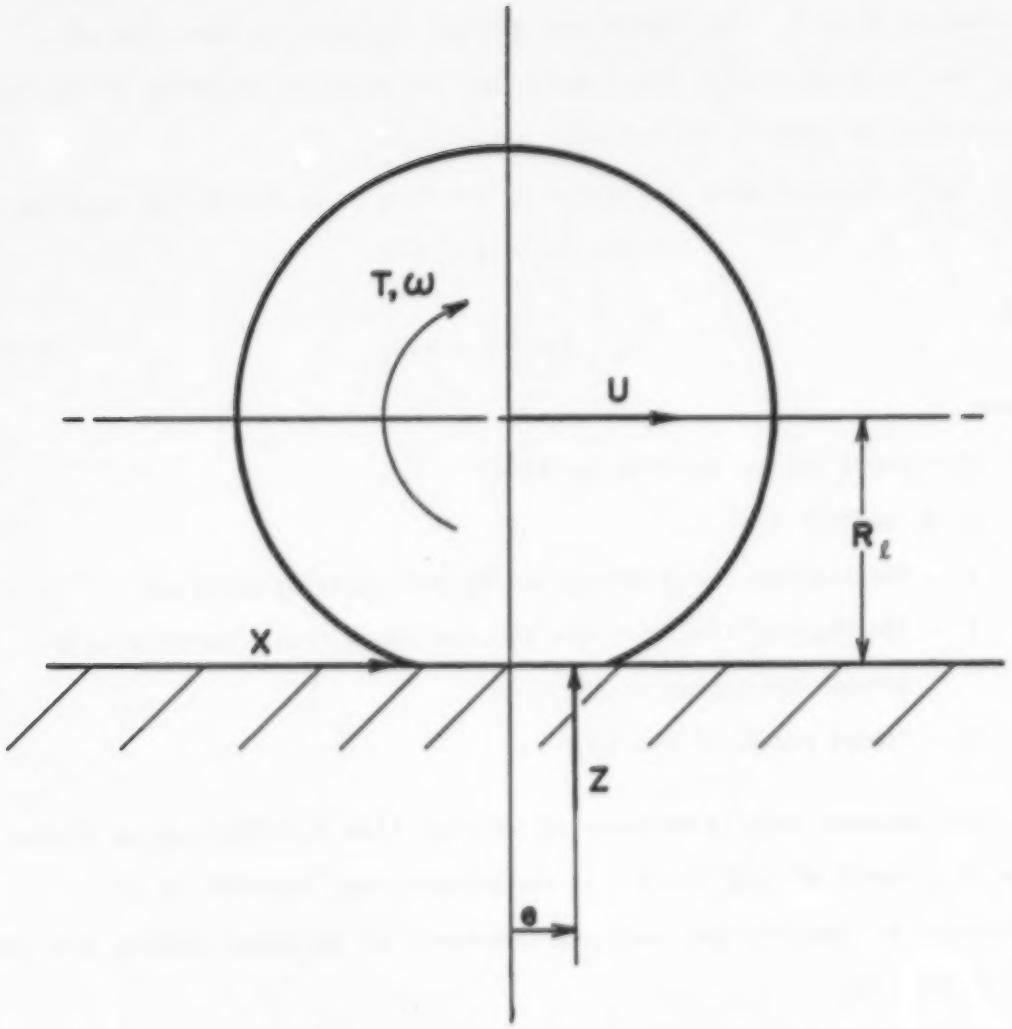

Figure B-1. Force and moment system acting on the tire. Torque (T) and longitudinal force (X) are positive when the tire is transmitting a driving torque.

P_S = power lost in the contact patch due to sliding between tire and pavement

= sink

where

ω = angular velocity of the tire

U = translational velocity of the axle

Assigning positive and negative signs to sources and sinks, respectively, gives the power equation:

$$T \cdot \omega - X \cdot U - P_I - P_S = 0 \qquad \text{(B-2)}$$

which is valid for both driving and braking because the signs of T and X change with the mode of operation.

The term P_I cannot be expressed with any certainty as a function of longitudinal tire slip and will be retained as an essentially unknown quantity. On the other hand, the term P_S can at least be expressed as a function of slip and the force (X_S) generated in the portion of the contact patch which is sliding.

Therefore, define longitudinal slip as [4]:

$$S = \frac{\omega \cdot R_e}{U} - 1 \qquad \text{(B-3)}$$

where

R_e = effective rolling radius and assume that the sliding velocity in the contact patch (where sliding is present) is constant and is given by:

$$\omega \cdot R_e - U = U \cdot S$$

then $$P_S = X_S \cdot U \cdot S \qquad \text{(B-4)}$$

Note that P_S is always positive because X_S and S always have the same sign.

Equation (3) can also be rearranged to give:

$$\omega = \frac{U(S+1)}{R_e} \qquad \text{(B-5)}$$

Now substitute equations (B-4) and (B-5) into equation (B-2); rearranging to solve for T

$$T = \frac{R_e}{U(S+1)} \left(X \cdot U + X_S \cdot U \cdot S + P_I\right)$$

And substitute for T in equation (1).

$$Z \cdot e = \frac{R_e P_I}{(S+1)U} + \frac{R_e X_S S}{(S+1)} + \frac{R_e X}{(S+1)} - R_\ell X$$

A simpler expression can be obtained by using:

$$X_S = X - X_A$$

where

X_A = force generated in that portion of the contact path which is not sliding.

$$Z \cdot e = \frac{R_e P_I}{(S+1)U} + (R_e - R_\ell)X - \frac{R_e X_A S}{(S+1)} \qquad \text{(B-6)}$$

For constant vertical force (Z), this equation gives the longitudinal position of the point of application of the vertical force. When slip (S) is zero, the longitudinal force (X) is equal to the free rolling (rolling resistance) force (X_R) and is negative. Also, the internal power loss is equal to the rolling resistance force times forward speed.

$$\text{for } S = 0,\ X = -X_R,\ \text{and } P_I = X_R U$$

$$\text{and } Z \cdot e = R_\ell \cdot X_R$$

Which is the normal expression for rolling resistance moment under free rolling conditions. It represents the only case in which the contribution of the internal power loss to the rolling moment (Z•e) can be stated explicitly, and then only if sliding in the contact patch is assumed to be negligible. Experimental evidence describing the variation of internal power loss with slip does not exist, although it is reasonable to suppose that some variation does occur. First, if forward speed is held constant, the power loss should change with angular velocity because of the change in the number of strain cycles experienced per unit time by each element of the tire. In the limiting case of locked wheel sliding, internal power loss in the tire is zero. Second, the strain cycle experienced by each tire element varies with transmitted torque. Other factors, such as temperature change, enter the problem as well. For example, sliding in the contact patch will increase the tread temperature, with an associated tendency to reduce internal losses. In view of these difficulties, the first term on the right hand side of equation (B-6) will be ignored from now on.

B.3 Variation of Rolling Moment with Slip

Two idealized cases of tire operation are often identified to simplify analysis of tire behavior: complete adhesion between the tread and pavement surface in the contact patch, and mixed adhesion and sliding in the contact patch. Also, the assumption of a linear relationship between longitudinal force and slip usually accompanies the assumption of complete adhesion. Each of the two cases is treated separately to give an indication of how the rolling moment varies with slip.

B.3.1 Complete Adhesion

Under this assumption, the relationship between longitudinal force and slip is:

$$X = C_S S$$
$$X_A = X \quad \text{and} \quad X_S = 0 \tag{B-7}$$

The rolling resistance force (X_R) is implicit in the term P_I of equation (B-6) and, since P_I has been dropped, must be omitted from the equation for longitudinal force. It should also be noted that slip is small when the tire is operating within the linear range. For the present purpose it can be considered to vary between ±0.05.

If $1/(S+1)$ is expanded as an infinite series, equation (B-6) rewritten as:

$$Z \cdot e = (R_e - R_f)X - R_e X(S - S^2 + S^3 - S^4 + \ldots)$$

Now substitute for S from equation (B-7)

$$Z \cdot e = (R_e - R_f)X - R_e\left(\frac{X^2}{C_S} - \frac{X^3}{C_S{}^2} + \ldots\right)$$

When $|S| = 0.05$, retaining only the first term in the series expansion leads to an error in the value of the expansion of less than 5%.

Therefore,
$$Z \cdot e = (R_e - R_\ell)X - R_e \cdot \frac{X^2}{C_S} \tag{B-8}$$

B.3.2 Mixed Adhesion and Sliding

The tire model of Reference [5] is used to indicate the trend of rolling moment behavior when sliding is present in the contact patch. Perhaps the most serious deficiency of the model as applied to the present problem is that longitudinal shear stress is assumed to vary linearly in the adhesion region, ignoring the antisymmetrical superimposed shear stress (present under free rolling conditions) and the effects of initial sliding as the tread elements enter the contact patch. The clear distinction made in the model between adhesion and sliding regions is thus not likely to hold in practice. Gross trends present in the behavior of the tire are, however, predicted by the model.

From Appendix A of [5], it can be shown that the adhesion component of longitudinal tire force, when sliding is present, is predicted by the model to be:
$$X_A = \frac{X_m^2}{4C_S} \cdot \frac{(S+1)}{S} \tag{B-9}$$

where

X_m = maximum shear force which can be generated by the tire.

$= \mu \cdot Z$

μ = coefficient of friction (assumed here to be constant with load and sliding velocity).

It can also be shown that the transition from complete adhesion to mixed adhesion and sliding occurs when:

$$|X| = \frac{X_m}{2}$$

Therefore, substituting for X_A in equation (B-6) from equation (B-9) gives:

$$Z \cdot e = (R_e - R_\ell)X - \frac{R_e X_m^2}{4C_S} \quad \text{when } |X| > \frac{X_m}{2} \qquad \text{(B-10)}$$

Equation (B-8) holds when $|X| < \frac{X_m}{2}$, and equations (B-8) and (B-10) are equal when $|X| = \frac{X_m}{2}$.

It should be noted that, apart from the truncation of the power series, a slight inconsistency does exist at the transition point since the model of Reference [5] predicts longitudinal force in the adhesion region to be

$$X = \frac{C_S S}{(S+1)} \text{ and not } X = C_S S$$

The (S+1) term in the denominator can be removed by taking the required integration in the derivation over a contact which varies in length as the total shear deformation instead of assuming that the contact length is constant. A slightly different expression is then obtained for equation (B-10). But the difference is minor, except when slip has a value close to unity, and is not important considering the other deficiences in the model.

B.4 Typical Results

Reference [6] presents a list of measured tire characterisitics which include the parameters required by equations (B-8) and (B-10). Table B-1 reproduces the appropriate values for a bias belted tire and a radial tire.

Figure B-2 shows the longitudinal tire force characteristics of the two tires as predicted by the model of Reference [5], assuming a coefficient of friction of 0.9 and a vertical load of 4.5 kN. Figure B-3 shows the rolling moment characteristics according to equations (B-8) and (B-10). Within the complete adhesion region ($|X|<X_m/2$) an inverted parabola can be seen superimposed on the straight line $(R_e - R_\ell)X$. Outside the region of complete adhesion, only a linear trend is evident, but again with slope $(R_e - R_\ell)$.

Reference [6] also presents measurements of rolling resistance moment (M_y), plotted against longitudinal force. One of the two graphs in the paper is reproduced in Figure B-4, where it can be seen that the data points are quite sparse around the origin, and that there is considerable scatter. A straight line fit was made through the curve (in the Reference) and a rolling resistance moment constant defined as the slope of the line. Values of the constant were given for the bias belted and radial tires. They are reproduced in Table B-1 together with values of $(R_e - R_\ell)$ for comparison. The term $(R_e - R_\ell)$ is approximately 50% greater than the rolling resistance moment constant for both tires, but it should be remembered that if the curve is indeed nonlinear, and taking into account the scatter in the data, then simple comparisons of this type could be misleading. It should also be remembered that internal tire losses were ignored when constructing Figure B-3.

Table B-1. Measured Tire Data, Abstracted From Reference 6

	Bias Belted H78-15	Radial HR78-15
Loaded radius of freely rolling tire, R_ℓ(cm)	35.1	32.6
Effective radius of freely rolling tire, R_e(cn)	36.3	34.7
Braking stiffness, C_S(kN)	87.0	160.0
Rolling resistance moment constant, k(cm)	.73	1.43
$(R_e - R_\ell)$, (cm)	1.2	2.1
$(R_e - R_\ell)/k$	1.64	1.47

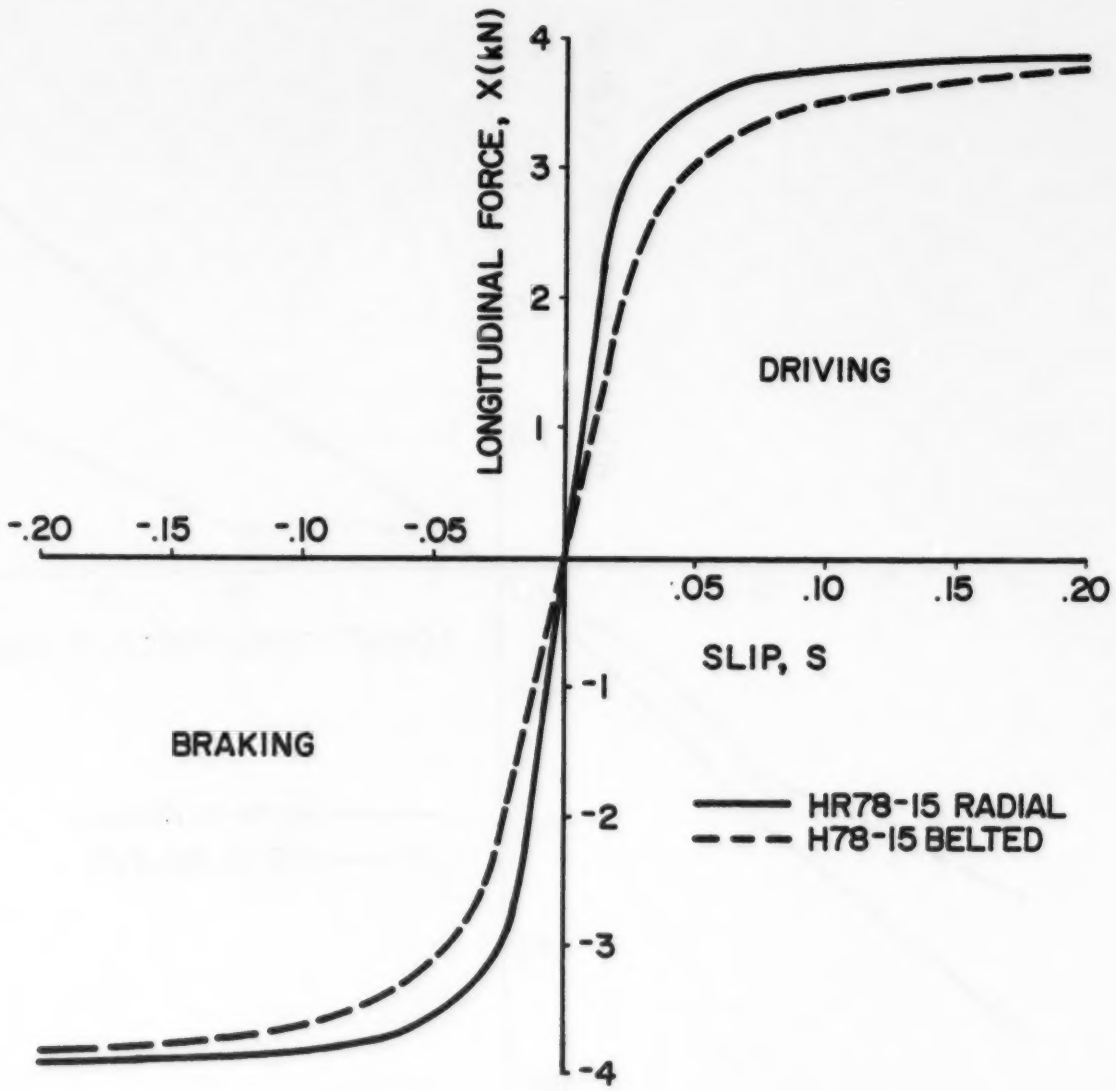

Figure B-2. Longitudinal force characteristics calculated from the tire model of reference (5) for the parameter values in Table B-1.

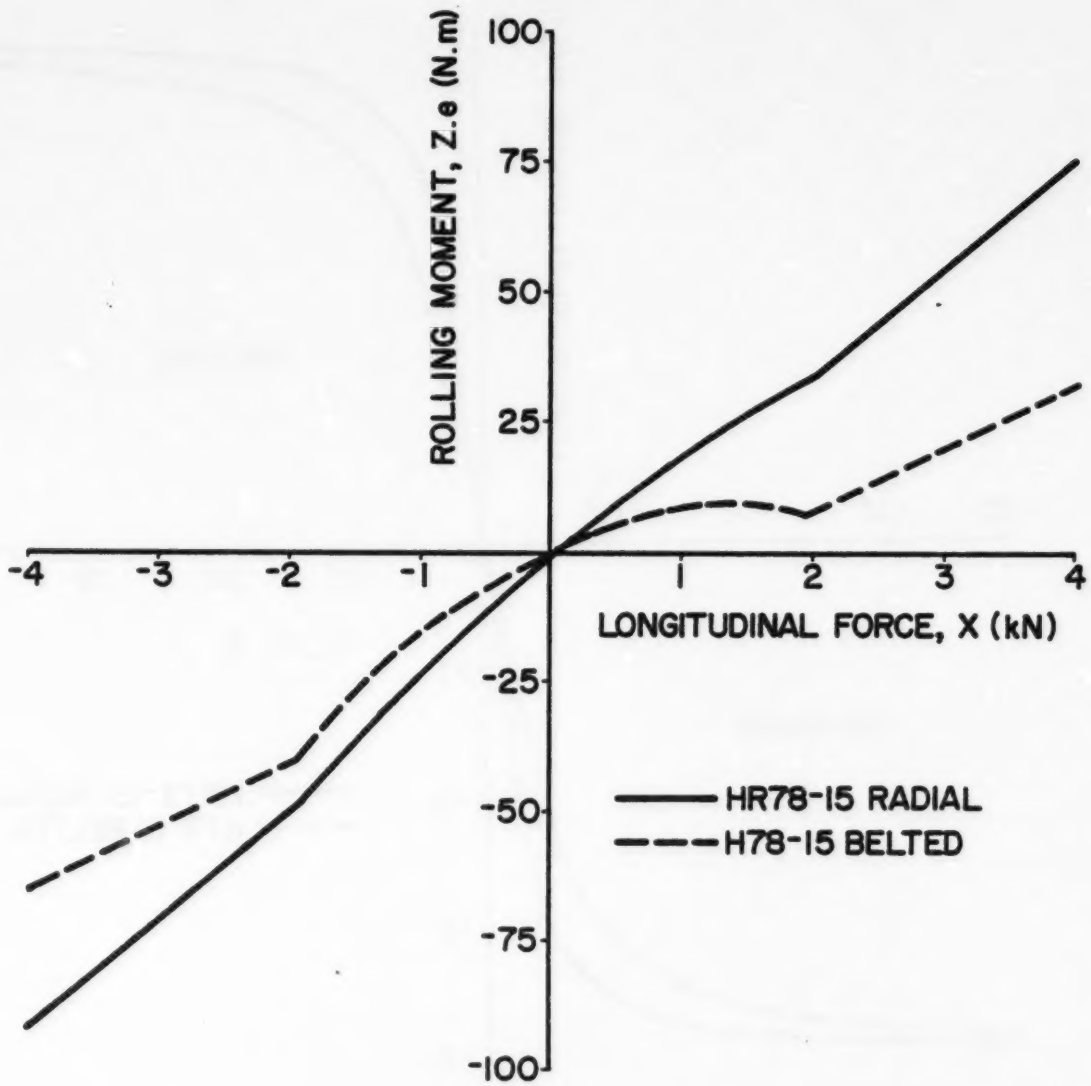

Figure B-3. Rolling moment calculated from equations (B-8) and (B-10) for the parameter values in Table B-1.

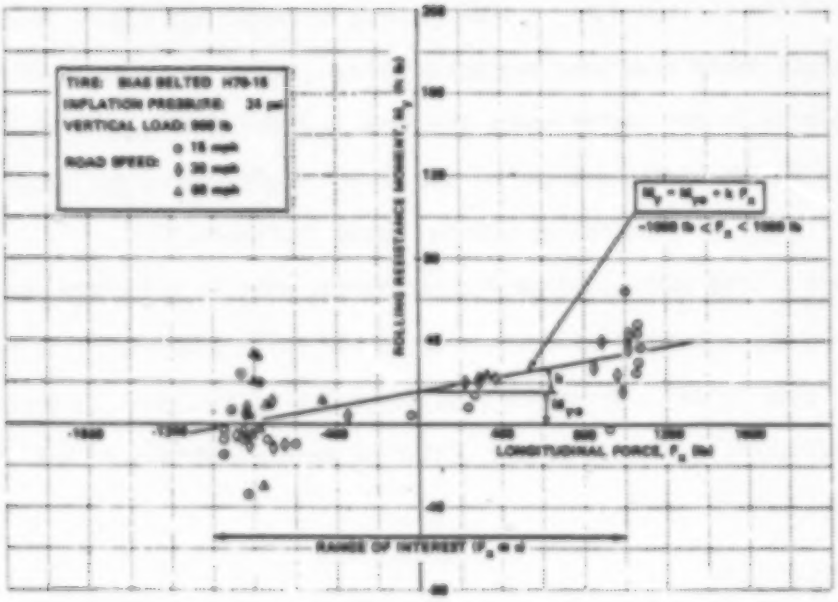
TIRE: BIAS BELTED H78-15
INFLATION PRESSURE: 24 psi
VERTICAL LOAD: 900 lb
ROAD SPEED: ○ 15 mph
◇ 30 mph
△ 60 mph
ROLLING RESISTANCE MOMENT, M_y (in lb)
LONGITUDINAL FORCE, F_x (lb)
$M_y = M_{yo} + k F_x$
$-1000 \text{ lb} < F_x < 1000 \text{ lb}$
M_{yo}
RANGE OF INTEREST ($F_x \approx 0$)

Figure 8-4. Rolling resistance moment for the bias belted H78-15 tire versus longitudinal force at 900 lb of vertical load.

(Figure and Caption from Reference [5].)

A later paper, Reference [2], presents a similar plot of rolling moment against longitudinal force, but for a different tire, under different load, and running on a wet surface. The graph is reproduced in Figure B-5, where is evident that the data points are distributed more regularly than in the previous figure, and that the scatter is much less. Excluding the extreme limits of the plotted data, a smooth curve drawn on the figure to connect the data points would show many characteristics similar to those of Figure B-3, particularly in the region where the tire is transmitting driving torque. The loop at the right hand end of the curve is presumably due to a reduction in coefficient of friction as sliding speed increases.

Very little other published experimental data is available which describes the characteristic behavior of the rolling moment for tires transmitting torque. Reference [7], for example, discusses in general terms the longitudinal movement of the center of vertical pressure, but gives no numerical values.

B.5 Conclusions

By purely analytical arguments, it has been shown that the rolling, or spin, moment acting on a tire which is transmitting torque is a complex function of the tires elastic and internal damping characteristics, and of the characteristics of relative sliding in the contact patch. It has also been shown that substantial variations in the rolling moment with driving torque will occur even for a tire which is assumed to have no internal (rolling) losses and where sliding in the contact patch is negligible. "Rolling resistance moment" therefore seems to be appropriate as a descriptive term only when a tire is freely rolling.

Comparison of computed results with a limited amount of experimental data taken from the published literature tends to confirm the basic validity of the mechanisms proposed and the models derived.

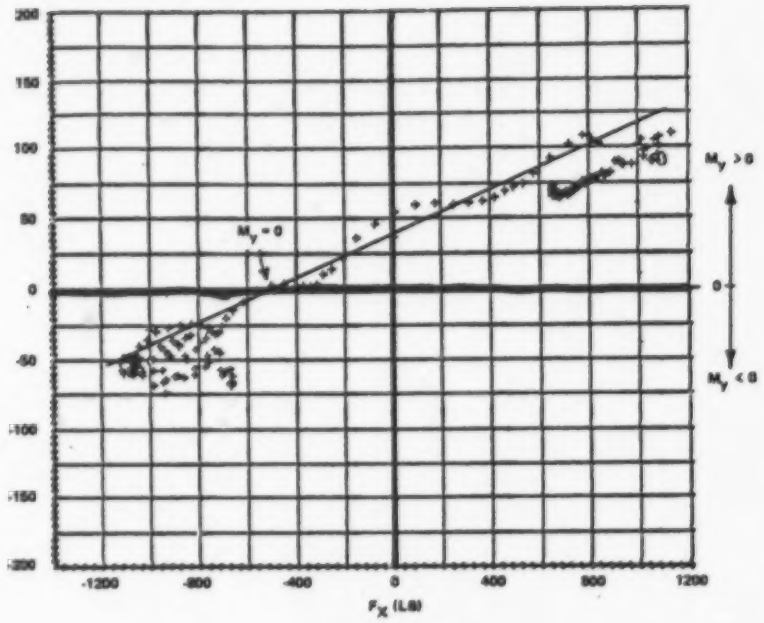

Figure B-5. Rolling resistance moment M_y versus longitudinal force F_x for a steel-belted GR78-15 (PC) radial tire under a vertical load F_z of 1500 lb (6.67 kN) on a wet surface. (Figure and Caption from Reference [1].)